

Tuning Polyamidoamine Design to Increase Uptake and Efficacy of Ruthenium Complexes for Photodynamic Therapy

Luca Mascheroni,^{1,2,†} Maria Vittoria Dozzi,¹ Elisabetta Ranucci,¹ Paolo Ferruti,¹ Valentina Francia,² Anna Salvati,^{2*} Daniela Maggioni^{1*}

¹ Dipartimento di Chimica, Università degli Studi di Milano, Via Golgi 19, 20133, Milan, Italy

² Groningen Research Institute of Pharmacy, University of Groningen, Antonius Deusinglaan 1, 9713AV Groningen, The Netherlands

Abstract

In this work, we report the synthesis of $[\text{Ru}(\text{phen})_3^{2+}]$ -based complexes and their use as photosensitizers for photodynamic therapy (PDT), a treatment of pathological conditions based on the photo-activation of bioactive compounds, which are not harmful in the absence of light irradiation. Of these complexes, Ru-PhenISA and Ru-PhenAN are polymer conjugates containing less than 5%, (on a molar basis), photoactive units. Their performance is compared with that of a small $[\text{Ru}(\text{phen})_3^{2+}]$ compound, $[\text{Ru}(\text{phen})_2\text{BAP}](\text{OTf})_2$ (BAP=4-(4'-aminobutyl)-1,10-phenanthroline, OTf=triflate anion), used as a model of the photoactive units. The polymer ligands, PhenISA and PhenAN, are polyamidoamines with different acid-base properties. At physiological pH, the former is zwitterionic and the latter moderately cationic, and both intrinsically cytocompatible. The photophysical characterizations show that the complexation to macromolecules does not hamper the $\text{Ru}(\text{phen})_3^{2+}$ ability to generate toxic singlet oxygen upon irradiation, and phosphorescence lifetimes and quantum yields are similar in all cases. All three compounds are internalized by HeLa cells and can induce cell death upon visible light irradiation. However, their relative PDT efficiency is different: the zwitterionic PhenISA endowed with the Ru-complex lowers the PDT efficiency of the free complex, while conversely, the cationic PhenAN boosts it. Flow cytometry demonstrates that the uptake efficiency of the three agents reflects the observed differences in PDT efficacy. Additionally, intracellular localization studies show that while $[\text{Ru}(\text{phen})_2\text{BAP}](\text{OTf})_2$ remains confined in vesicular structures, Ru-PhenISA localization is hard to determine due to the very low uptake efficiency. Very interestingly, instead, the cationic Ru-PhenAN accumulates inside the nucleus in all treated cells. Overall, the results indicate that the complexation of $[\text{Ru}(\text{phen})_2\text{BAP}](\text{OTf})_2$ with a cationic polyamidoamine to give the Ru-PhenAN complex is an excellent strategy to increase the Ru-complex cell uptake and, additionally, to achieve accumulation at the nuclear level. These unique features together make this compound an excellent photosensitizer with very high PDT efficiency.

Keywords: photodynamic therapy, ruthenium complexes, linear polyamidoamines, cell uptake, flow cytometry, confocal microscopy, nanomedicine.

1. Introduction

In recent years, photodynamic therapy (PDT)¹ has drawn increasing attention for its potential as an alternative or adjuvant treatment for several solid tumours,^{2,3} for instance skin, bladder, esophagus or lung tumours.⁴ Although still emerging, PDT is already a successful clinically approved therapeutic modality for the treatment of neoplastic and other non-malignant diseases.^{5,6} The major innovation of PDT relies on the use of two agents, the photosensitizer (PS) and light, negligibly toxic if administered independently, but remarkably so if jointly administered. Whereas the former might locally accumulate also in healthy tissues, the second can be specifically directed to pathological tissues. Therefore, PDT is expected to cause less severe side effects than chemotherapy, since possible photosensitizer accumulation in healthy tissues would not be harmful unless irradiated. Moreover, it has been observed that the effect of PDT treatment is not only limited to the cancerous mass itself, but it also extends to the surrounding endothelial tissue, causing a halt in the perfusion of a tumour that contributes to its total clearance and prevents cases of relapse.^{7,8}

Photo-induced damage generated by PDT may be due to several photochemical reactions that can occur on the bases of two different kinds of molecular mechanisms. Initially, the light radiation activates the PS, which may interact with H₂O, O₂ or a biological substrate forming different kinds of reactive oxygen species (ROS). In particular, the first path is based on an electron transfer mechanism and promotes the production of hydroxyl radical anion HO[•] and/or superoxide radical anion O₂^{•-} (type I PDT). The second path mainly consists in the direct conversion of molecular oxygen from its triplet ground state ³O₂ to singlet oxygen excited state ¹O₂ through an energy transfer mechanism (type II PDT). Type II is the most relevant PDT mechanism in cells, since most PSs are effective producers of ¹O₂, which is known to be a highly cytotoxic species, and inside living cells, it can cause damage to mitochondria, the Golgi apparatus, endoplasmic reticulum, lysosomes and endosomes, as well as nuclei. The cellular damage caused by singlet oxygen often leads to cell death that, in most cases, occurs via the apoptotic pathway (also known as programmed cell death).⁹ While the type II PDT mechanism dominates in oxygenated tissues, the type I PDT can also occur in hypoxic tissues.^{10,11}

Some of the major bottlenecks for the employment of PDT in clinics are the poor efficiency of visible light to penetrate soft and hard tissues in order to activate the photosensitizer and issues related to the delivery efficiency of the photosensitizer into the targeted area. Given the limits in tissue penetration, PDT has so far been adopted mainly for the treatment of skin diseases.² The main challenge of recent years has been the design of PDT agents capable of absorbing radiations in the 620-850 nm spectral region, the so-called “optical window” in which human tissues show the highest transmittance, while maintaining the requirements of clinical photosensitizers, that is, negligible toxicity at the therapeutic concentrations, photo-bleaching

resistance and stability in physiological environments.¹ Photosensitizers belonging to the porphyrin- and phthalocyanine families are currently used for PDT, but their therapeutic efficacy is limited by the poor solubility and the tendency to self-aggregation.¹⁰ Promising alternatives are metal-based photosensitizers, that is, coordination compounds of transition metals capable to excite the ground state molecular oxygen through the mechanisms mentioned above,¹² making them potential PDT agents.¹³ On top of this, metal-based photosensitizers typically show several advantages compared to their organic counterparts: high photo-stability, high quantum yields of triplet formation, long lifetimes, tunable excitation and emission by virtue of their first-sphere coordinating ligands, and finally, the potential to be excited also by two-photon absorption (TPA).¹⁴

Among many coordination compounds, ruthenium (II) complexes have promising features as PSs.^{13,15-18} Interestingly, they can be excited by both one-photon and two-photon excitation mechanisms,^{12,19-21} the latter usually exploiting the long-lived triplet metal-to-ligand charge transfer state (³MLCT). In particular, Ru(II)-polyimine complexes bearing three chelating phenanthroline ligands, Ru(phen)₃²⁺, can act as PS and can interact with DNA minor grooves.²² If extended planar ligands are introduced in the Ru coordination sphere, the photoactive complex can act as a nucleus/DNA targeting agent by effectively intercalating DNA and work as a "light switch".²³⁻²⁷ More importantly, one Ru(II)-based PS, the TLD1433, has already reached the human clinical trials, and its development is described in ref. 13.

Next to the development of novel photosensitizers with improved optical properties, recently, the use of nanoparticles has been proposed as an ulterior strategy to improve the success of PDT by improving the photosensitizer delivery^{9,28} by increasing their solubility, biocompatibility, and PS biodistribution to the target. The latter is strictly related to the size of nanomaterials, which tend to accumulate in tumor masses by passive targeting via the so-called enhanced permeability and retention (EPR) effect.^{29,30}

Among multiple nanomaterials under study, polymers play a role in the encapsulation of Ru-based anticancer drugs or antibacterial agents, as recently reviewed in details by Villemin et al.³¹ Also the incorporation of luminescent Ru complexes into peptides has been deeply investigated (see review 18 and refs. therein). Polyamidoamines (PAAs) are linear synthetic polymers with several favourable characteristics for their use in biomedicine,^{32,33} especially as drug carriers.³⁴⁻³⁸ They have been shown to enter all cell types in which they have been tested, including among others HEK 293 cells,³⁹ 3T3 clone A31 cells,⁴⁰ PC3 cells,³⁸ and B16F10 cells.⁴¹ Most of them are soluble in water, biocompatible and biodegradable. Moreover, they are endowed with exceptional structural versatility. In particular, they can be easily functionalized by inserting side chains that carry specific moieties to link biologically active functions and/or modulate their overall physical and chemical properties.³² They are also amenable to exhibit EPR effect.⁴²

Here, two polymer conjugates based on PAAs have been designed, Ru-PhenISA and Ru-PhenAN (Chart 1), characterized by a different global charge at physiological pH. We have studied the cell uptake efficiency and PDT efficacy of the two macromolecular complexes, and compared them with the results for the cationic

molecular Ru-complex $[\text{Ru}(\text{phen})_2\text{BAP}](\text{OTf})_2$ (Chart 1), used as a model of the photoactive units. Subcellular localization and dark/light cytotoxicity of the three Ru-complexes have been analyzed, correlating the cell mortality levels induced by irradiation to the different behavior at the cell level, and in this way, enabling us to select the PS with the most promising properties for PDT.

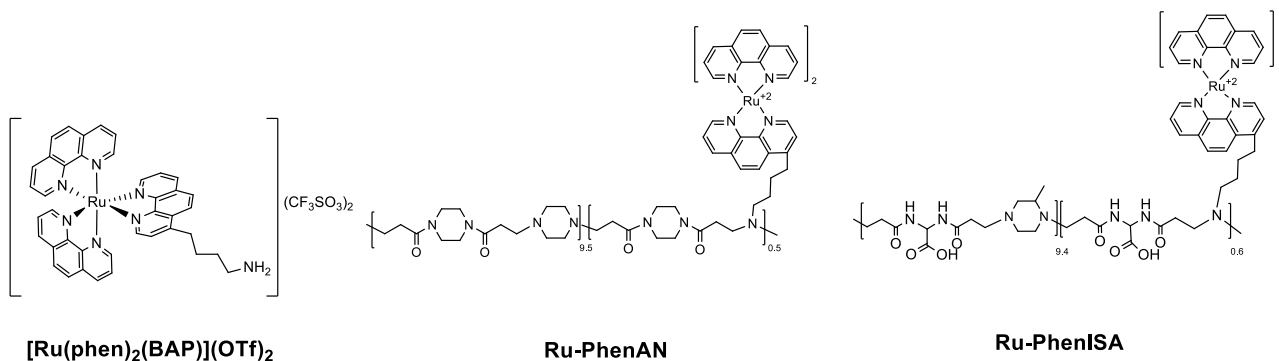
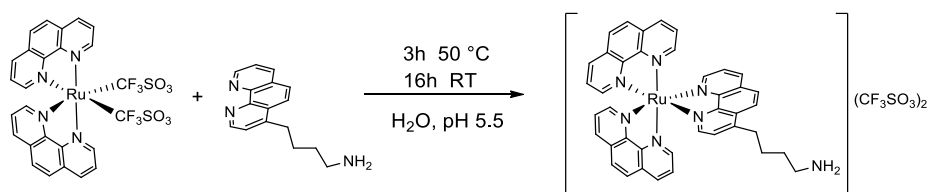


Chart 1. Schematic depiction of the three Ru derivatives.

2. Results and discussion

Modification of the Ru-complex $\text{Ru}(\text{phen})_2\text{BAP}^{2+}$ with either a zwitterionic or cationic polymer is likely to strongly affect the resulting interactions with cells. For this reason, we have prepared first of all the molecular Ru complex and then we have conjugated it to the PAAs PhenISA and PhenAN with less than 5% photoactive units (on a molar basis). The main portion of PhenISA and PhenAN polymers corresponds to two previously synthesized PAAs, named ISA23,⁴³ and BP-P,⁴⁴ respectively. The two PAA chains differ as regards acid-base properties: BP-P is moderately cationic, with approximately 0.5 positive charges per repeat unit at pH 7.4; ISA23 is amphoteric with isoelectric point ~ 5.2 , with approximately 0.4 negative charges per repeat unit at physiological pH.⁴⁵ PhenISA has been previously employed as a chelating agent for rhenium (Re-PhenISA), ruthenium (Ru-PhenISA)³⁹ and iridium (Ir-PhenISA),⁴⁶ Ir-PhenISA has been already investigated as a singlet-oxygen sensitizer for photodynamic therapy.⁴⁶ Since it has been suggested that cationic PAAs may enter cells more eagerly than anionic ones,⁴¹ next to the amphoteric prevalently anionic Ru-PhenISA we have prepared the moderately cationic Ru-PhenAN.

2.1 Synthesis of the molecular complex $[\text{Ru}(\text{phen})_2\text{BAP}](\text{OTf})_2$. $[\text{Ru}(\text{phen})_2\text{BAP}](\text{OTf})_2$, chosen as a model of the photoactive repeat units was obtained from the reaction of $\text{Ru}(\text{phen})_2(\text{OTf})_2$, containing two labile triflate anions, with 4-(4'-aminobutyl)-1,10-phenanthroline (BAP), as reported in Scheme 1.



Scheme 1. Schematic representation of the synthesis of $[\text{Ru}(\text{phen})_2(\text{BAP})](\text{OTf})_2$

We carried out the reaction in water to avoid contamination by possibly noxious organic solvents at 55 °C, and importantly, to mimic the reaction of the ruthenium precursor with the two polyamidoamines, which are soluble only in water. The orange luminescence of the reaction mixture, by irradiation at 366 nm, confirmed the progress of the reaction. ^1H NMR analysis indicated after 3 h the presence of only 5% unreacted $\text{Ru}(\text{phen})_2(\text{H}_2\text{O})_2^{2+}$ (Figure S1), which remained unchanged also after another reaction night at room temperature. The raw product was purified raising pH to 11.5 and eliminating the unreacted precursor that precipitated as the dihydroxide $\text{Ru}(\text{phen})_2(\text{OH})_2$ complex. The complete NMR characterization of $[\text{Ru}(\text{phen})_2\text{BAP}](\text{OTf})_2$ is reported in the Supporting Information (Figures S2 and S3). Purified $[\text{Ru}(\text{phen})_2\text{BAP}](\text{OTf})_2$ was maintained in aqueous solution, adjusting the pH at ~ 7 , and its concentration (4.14 mM) determined by UV-vis spectroscopy, assuming a molar extinction coefficient at 450 nm equal to that of $\text{Ru}(\text{phen})_3^{2+}$ in water ($\epsilon_{450\text{nm}}=19200 \text{ M}^{-1}\cdot\text{cm}^{-1}$).⁴⁷

2.2 Synthesis and characterization of Ru-PhenISA. We synthesized Ru-PhenISA according to a previously published two-step procedure,³⁹ (see scheme in Figure 1a). The first step consisted in the synthesis of PhenISA by co-polyaddition of 2-methylpiperazine and BAP with 2,2'-bis(acrylamide)acetic acid. Thanks to its primary amine group, BAP participated in the polyaddition reaction with the bisacrylamide thus introducing butylphenanthroline pendants to PhenISA main chain that in this case was $\sim 4\%$ (based on ^1H NMR analysis). In the second reaction step, the phenanthroline pendants were reacted with $\text{Ru}(\text{phen})_2(\text{TfO})_2$ obtaining $[\text{Ru}(\text{phen})_3]^{2+}$ groups as lateral substituents linked via butyl segments to the PAA chain (Figure 1a and Experimental Section for details).

We carried out DLS measurements for determining the state of aggregation of this polymer complex. Indeed, linear polyamidoamines tend to self-assemble in aqueous solution, giving nano-aggregates of variable size,^{32,46,48} and making their characterization sometimes complicated. This behavior can be ascribed to different weak interactions, depending on the composition of the polymer coils, such as hydrogen bonds, electrostatic interactions and, in the case of PAAs bearing apolar pendants like cholesterol molecules⁴⁹ or phenanthrolines,⁴⁶ also hydrophobic interactions. DLS analysis showed three distinguishable distribution graphs (Figure 1b) centered at ~ 10 , 50 and 350 nm, the most relevant of which was the smallest one, as indicated by the volumes size distribution analysis (Figure 1c). On the bases of these results, we concluded that the Ru-PhenISA complex self-assembled in nano-aggregates with a mean hydrodynamic diameter of 10 nm in water, and only a negligible mass fraction (the volumes size distribution reflects the mass percentage present in each population) contributed to bigger aggregates.

As previously stated, at physiological pH PhenISA is zwitterionic with, on average, 0.4 negative charges per repeating unit. We determined the pH-dependence of PhenISA ζ -potential (Figure 1d). As expected, at the isoelectric point (pH ~ 5), the ζ -potential is zero, which represents a globally neutral particle surface, whereas at physiological pH the ζ -potential value is negative.

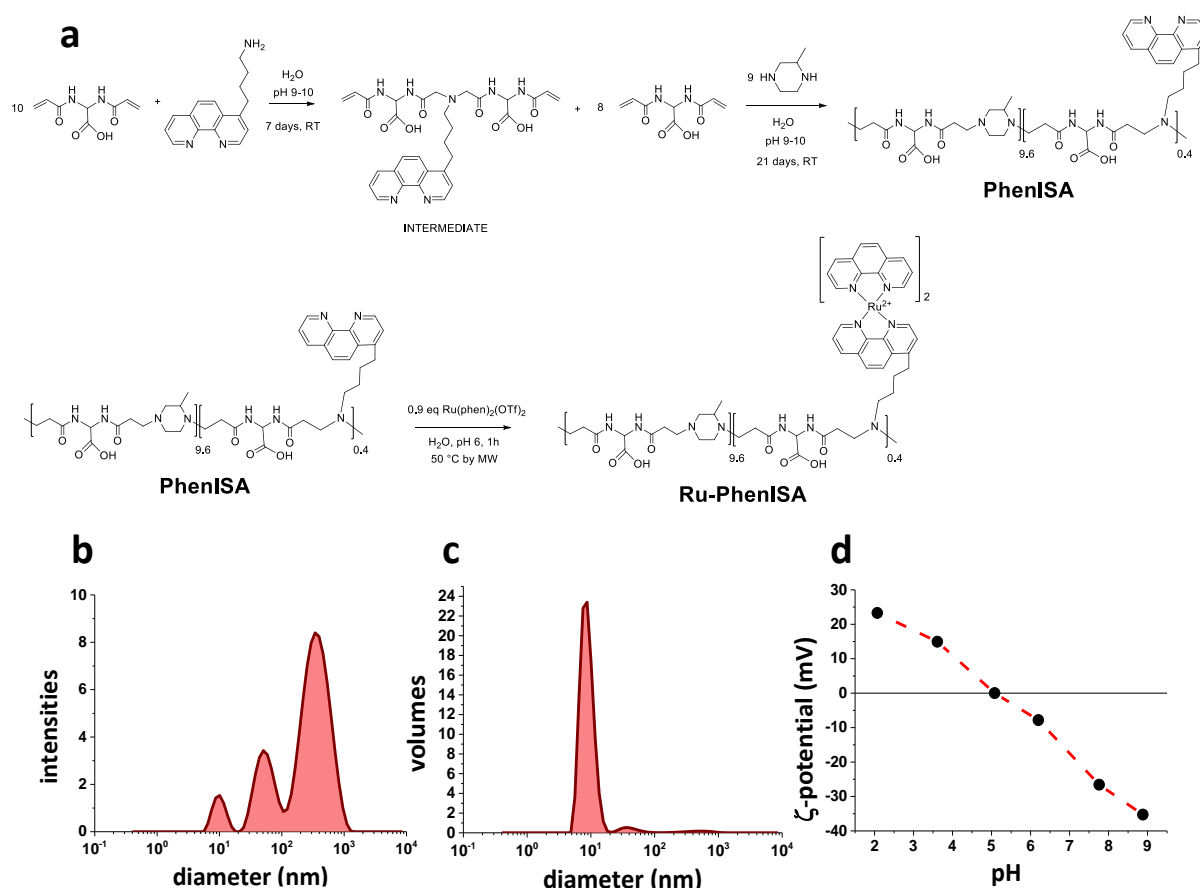


Figure 1. Synthesis and characterization of the copolymer PhenISA. a) Sketch of the synthesis of PhenISA copolymer and its derivative Ru-PhenISA; b) DLS measurements by intensities and c) by volumes; a) ζ -potential variation in water vs. pH.

2.3 Synthesis and characterization of PhenAN and its derivative Ru-PhenAN. In a previous paper, a PAA homopolymer deriving from the polyaddition of 2-Me-piperazine to 1,4-bis(acryloyl)piperazine (similar to the major component of the PhenAN copolymer) was found to be water-soluble and biocompatible.⁴⁴ Furthermore, it proved amenable to pH-dependent hydrolytic degradation in aqueous solution to non-toxic products. In particular, at 37 °C, it completely degraded within a few weeks at physiological pH, but was considerably more stable at lower pH inside lysosomes (5.0/5.5).⁵⁰ These features prompted us to investigate the feasibility of the synthesis of a copolymer with the same properties, and with the additional ability to bind metal moieties. This was achieved by inserting chelating phenanthroline pendants in the minor repeating units, thus obtaining a luminescent polymer complex.^{39,46}

The synthesis of the cationic copolymer PhenAN occurred through Michael polyaddition reactions of the double bonds of 1,4-bis(acryloyl)piperazine with the secondary amines of piperazine and the primary amine of 4-butylamino-1,10-phenanthroline (BAP) in ratio 10:9:1, respectively (see Scheme in Figure 2a). We stopped the reaction when a honey-like consistency was observed, and we purified by ultrafiltration. The number (M_n) and weight (M_w) average molecular weights of the product, as measured by size exclusion chromatography (SEC) analysis were 34630 and 48050, respectively (polydispersity index = 1.38).

Bases of ^1H NMR integrated intensities, we estimated the percentage of phenanthroline units as 4.5%, in front of the theoretical 10% in the feeding (see Supporting Information Figures S4-S8 and Table S1 for details and signal attributions).

We determined the averaged acidity constants of PhenAN piperazine units ($\text{pK}_{\text{a}1} = 3.35$; $\text{pK}_{\text{a}2} = 7.40$, Figure S9) by potentiometric titration^{45, 51} (the values are in line with what reported for related piperazine-containing PAAs,⁴⁵ and are lower than those measured for free piperazine ($\text{pK}_{\text{a}1} = 5.35$; $\text{pK}_{\text{a}2} = 9.73$) and for 1,4-dimethylpiperazine ($\text{pK}_{\text{a}1} = 3.81$; $\text{pK}_{\text{a}2} = 8.38$)⁵² due to the presence of the beta-C(O)NR₂ amide substituent). Therefore, on the average, the piperazine moieties bear 0.5 positive charge at pH 7.4 and one positive charge at lysosomal pH 4.5 (see the speciation diagram in Figure S9 of the Supporting Information). This is in line with the observed pH-dependence of the ζ -potential values (Figure 2d).

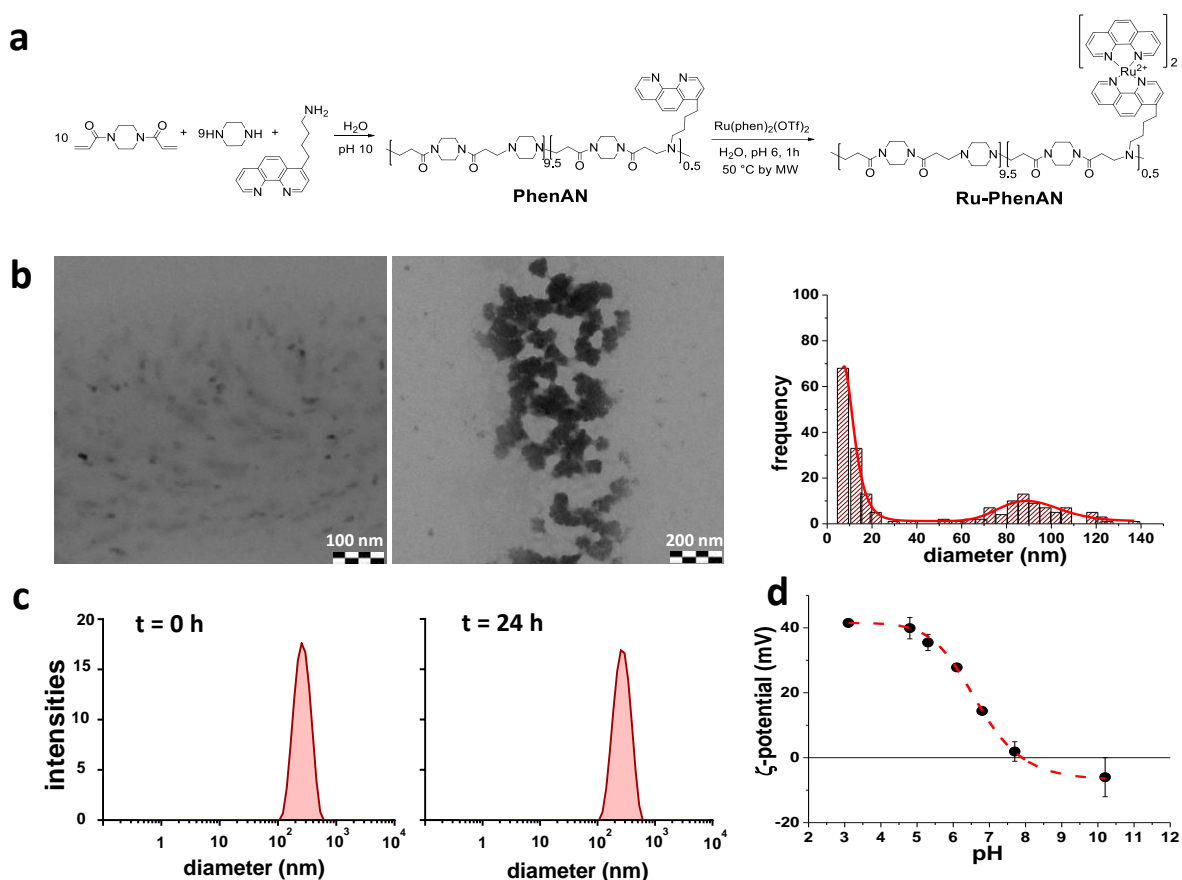


Figure 2. Synthesis and characterization of the copolymer PhenAN. a) Sketch of the synthesis of PhenAN copolymer and its derivative Ru-PhenAN; b) Representative bright field TEM images of PhenAN copolymer (left), and corresponding TEM size distribution (right); c) DLS size distribution (intensity profiles, NaCl 0.150 M solution) of PhenAN copolymer at its natural pH (3.5) at different observation times (0 and 24 h after dispersion), and (d) its ζ -potential titration curve as a function of pH (right).

We considered that these milder cationic properties could be advantageous to achieve an ideal cellular behavior: thanks to this design, and in particular the different pK_{a} values of the piperazine amine groups in the polymer, the positive character of the PhenAN coils in physiological conditions would be small enough to limit toxicity, but ideally still important to enable endosomal escape at the cellular level. In fact, even at the

lowest intracellular pH (~4.5 in the lysosomes), one of the two amine groups remains mainly unprotonated, in contrast to what observed with some of the most widely used polycationic transfecting agents, such as PEI⁵³ or polylysine,⁵⁴ which show a higher protonation degree already at pH 7, usually associated to higher toxicity.⁵⁵

In order to determine the size of the polymer, we used transmission electron microscopy (TEM) and dynamic light scattering (DLS).

Transmission electron microscopy showed nano-aggregates of about 80-100 nm, together with many much smaller structures (10-20 nm, Figure 2b). The analysis of the size distribution indicated that most of the NPs had a diameter smaller than 20 nm (maximum peaked at 9.2 ± 0.2 nm), with a lower fraction of aggregates with a mean diameter centered at 91 ± 2 nm. DLS of the polymer in saline water showed a mean hydrodynamic diameter of about 200 nm (by intensities, Figure 2c left) which remained stable also 24 h after the dissolution of the lyophilized polymer, indicating good stability of the aggregates over time (Figure 2c right). Smaller objects corresponding to the 20 nm diameter fraction observed at TEM were not detected by DLS. This is likely due to known DLS limitations for samples composed by soft materials (with a small scattering ability), and, most importantly, for polydisperse samples, given the much higher scattering ability of larger particles with respect to the smaller ones ($I \propto r^6$). Overall, we can conclude that the polymer is rather stable in solution, and once dispersed in aqueous solutions, it includes a large fraction of small objects around 20 nm and a smaller fraction of aggregates of around 100-200 nm.

Thus, we carried out the synthesis of the polymeric complex Ru-PhenAN by reacting PhenAN with the $[\text{Ru}(\text{phen})_2(\text{OTf})_2]$ precursor, under microwave irradiation in water (see Scheme in Figure 2a). The ^1H NMR spectrum (Figure S10), performed on the dialyzed sample, showed the expected resonance pattern for the Ru-PhenAN complex in the aromatic region. The aromatic resonances have been assigned by a scalar correlation experiment (Figure S11). To confirm the tight binding of the Ru fragment to the BAP pendant, we performed a ^1H DOSY NMR experiment, which showed the same diffusion coefficient for all the protons of the Ru-PhenAN complex (Figure S12). The Ru-containing polymer was ~ 2% of the repeat units. This value derived from two distinct complementary analyses: the number average molecular weight M_n from size exclusion chromatography (SEC) and elemental analysis (see Experimental Part and note 56). This means that not all the phenanthroline pendants (~ 5% from ^1H NMR) were coordinated to a $\text{Ru}(\text{phen})_2^{2+}$ moiety.

The concentration of Ru per polymer mass in a known water volume was confirmed by UV-vis spectroscopy on the same sample of lyophilized polymeric, based on the absorbance value of the maximum of $^1\text{MLCT}$ band (see Experimental Part for details).

2.4 Photophysical characterization of the Ru complexes. As a next step, we characterized photophysically the three Ru complexes. The absorption and emission profiles of $[\text{Ru}(\text{phen})_2\text{BAP}](\text{OTf})_2$, Ru-PhenISA and Ru-PhenAN are shown in Figure S13. The comparison of the spectra of the three species showed that both the

typical metal-to-ligand-charge-transfer ($^1\text{MLCT}$) absorption and the broad emission bands with maxima at ~ 610 nm closely resemble each other, and are also very similar to those of other $[\text{Ru}(\text{phen})_3]^{2+}$ complexes.⁵⁷

The UV-vis spectra of Ru-PheAN and Ru-PhenISA are dominated at low wavelengths by the strong absorption peaks of the amide groups of the polymer backbone, which partly overlap the $\pi\text{-}\pi^*$ transitions of the phenanthroline BAP. Of the latter, only the transition at higher wavelengths is recognizable, with a maximum at 270 nm at pH 7.

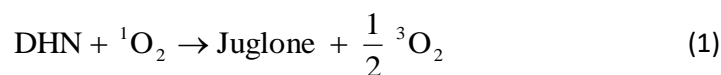
The photophysical data for the three compounds are shown in Table 1. Interestingly, we observed a slight increase in both lifetimes and quantum yields for both polymeric complexes compared to $[\text{Ru}(\text{phen})_2(\text{BAP})](\text{OTf})_2$. This could be ascribed to a slight shielding action of the polymer chains hindering the interaction between the triplet state emitting Ru complex and molecular oxygen. Molecular oxygen is in fact known to act as an important collisional quencher for phosphorescent species by facilitating non-radiative transitions to the ground state.

Table1. Photophysical data in aerated water solutions of the three Ru derivatives.

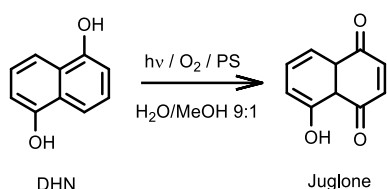
Compound name	$\lambda_{\text{abs MLCT}}$ (nm)	λ_{exc} (nm)	λ_{em} (nm)	τ (ns)	Φ %
$[\text{Ru}(\text{phen})_2(\text{BAP})](\text{OTf})_2$	425	450	612	492	2.5
	446				
Ru-PhenISA ^a	413	450	614	580	4.1
	442				
Ru-PhenAN	419	450	608	533	3.6
	448				

^a Data reported in Ref. 39

Photoreaction of the indirect reporter of singlet oxygen 1,5-Dihydroxynaphthalene with the Ru-based photosensitizers complexes. Before moving on to the biological assays, we then assessed the ability of the three synthesized compounds to generate singlet oxygen. The ability of the Ru complexes to generate singlet oxygen was assessed by using 1,5-dihydroxynaphthalene (DHN) as an indirect reporter of $^1\text{O}_2$ presence. DHN reacts promptly and quantitatively with $^1\text{O}_2$ forming the oxidized species Juglone (5-hydroxy-1,4-naphthalenedione, Scheme 2),⁵⁸ according to equation 1:



The conversion of DHN to Juglone can easily be monitored via UV-vis spectroscopy, following the decrease of the DHN absorption band at λ_{max} 297 nm and the concomitant increase of the broad Juglone absorption band centred at 427 nm (Figure 3).



Scheme 2. Photochemical conversion of DHN to Juglone.

We performed the experiments by mixing a methanol DHN solution with a water solution of the sensitizer (either $[\text{Ru}(\text{phen})_2(\text{BAP})](\text{OTf})_2$, Ru-PhenAN and Ru-PhenISA), which after being saturated with O_2 , was irradiated for a total time of 5-7 min by recording absorption spectra after every 1 min irradiation time. With the main aim to comparatively evaluate the quantum yields of singlet oxygen production of the three newly synthesized compounds, an extra experiment was performed by employing tris(bipyridine)ruthenium(II), labeled as $[\text{Ru}(\text{bpy})_3]\text{Cl}_2$, as reference sensitizer whose $^1\text{O}_2$ generation quantum yield in water is 0.41.³⁹

In a previous work with Ir-PhenAN complex, negligible Juglone formation was observed upon DHN irradiation in the absence of sensitizers.⁴⁶ Moreover, the possible formation of long-lived intermediates or by-products seems to be excluded because two isosbestic points at ca. 280 and 330 nm are observed in the spectra recorded at different times during irradiation. By considering the relatively short reaction time and the instantaneous interaction between DHN and $^1\text{O}_2$ to produce Juglone, we can thus apply the steady-state approximation to the $^1\text{O}_2$ intermediate species. Therefore, its formation rate coincides with its disappearance rate and can be related to the rate of DHN consumption, which is assumed to be first order in DHN,^{46,59} as reported below (equation 2).

$$r = \frac{d[{}^1\text{O}_2]}{dt} = -\frac{d[{}^1\text{O}_2]}{dt} = -\frac{d[\text{DHN}]}{dt} = k_{\text{obs}} [\text{DHN}] \quad (2)$$

Thus, by considering that under the selected experimental conditions the absorbance at 297 nm (A_{297}) can be exclusively ascribed to DHN, we can evaluate the rate constants (k_{obs}) of the DHN photo-oxidation process by fitting the A_{297} experimental data as follows (equation 3):

$$\ln \frac{[\text{DHN}]_t}{[\text{DHN}]_0} = \ln \frac{(A_{297})_t}{(A_{297})_0} = -k_{\text{obs}} t \quad (3)$$

The first-order semi-logarithmic plots for DHN photo-oxidation in the presence of the investigated sensitizers are shown in Figure 3, i.e. the $\ln(A_t/A_0)$ values linearly decrease all over the monitored irradiation time, in agreement with pseudo-first-order kinetics for all the investigated sensitizers.

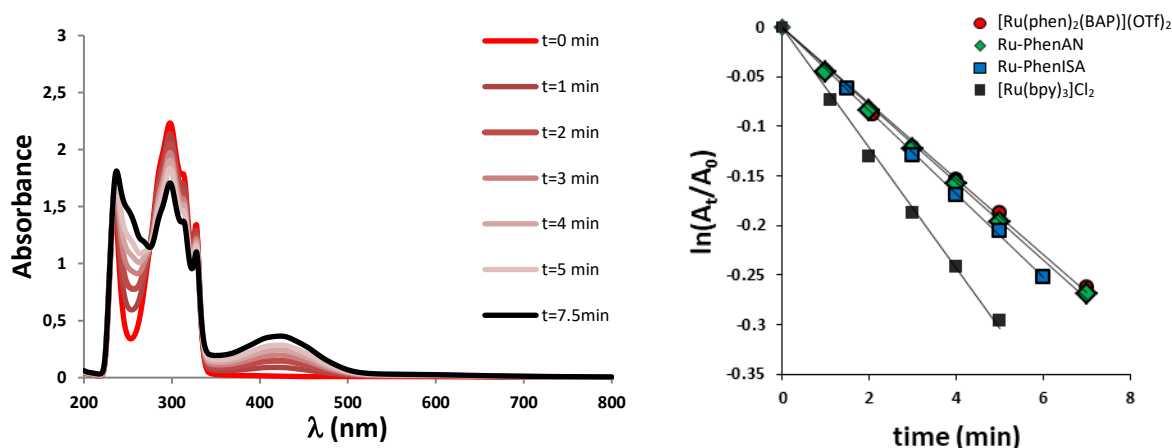


Figure 3. Left: Evolution of absorption spectra of H₂O/MeOH 9:1 solutions containing Ru-PhenAN (1.1·10⁻⁵ M of Ru) and DHN (3.3·10⁻⁴ M) irradiated for different times ($\lambda > 390$ nm), acquired by using as blank reference the solution containing only Ru-PhenAN species. Right: semi-logarithmic plots of ¹O₂ generation vs. the time for the sensitizers detected by DHN photo-oxidation.

We thus calculated the quantum yields of singlet oxygen generation (Φ_{Δ}) by using the following equation 4:

$$\Phi_{\Delta} = \Phi_{\Delta}^{\text{std}} \cdot \frac{v_i \cdot I^{\text{std}}}{v_{\text{std}} \cdot I} \quad (4)$$

where v_i is the initial rate of reaction 1, I indicates the photons absorbed by the sensitizer, and the std labels the corresponding values for the standard (Ru(bpy)₃²⁺ in our case, $\Phi_{\Delta}^{\text{std}} = 0.41$ in water). The values of v_i were obtained as the product $k_{\text{obs}} \cdot [\text{DHN}]_0$ (with $[\text{DHN}]_0$ being 3.3·10⁻⁴ M), while the values of I were estimated by numerical integration of $I_{\text{source}}(\lambda) (1 - 10^{-A(\lambda)})$, where $I_{\text{source}}(\lambda)$ is the intensity of the incident light at different wavelengths and $A(\lambda)$ is the corresponding absorbance of the considered sensitizer.

All the so calculated Φ_{Δ} values are collected in Table 2. Overall, the photophysical data indicated that the three derivatives had comparable UV-vis absorption behavior and, importantly, comparable capacity to produce singlet oxygen, showing similar Φ_{Δ} values both when the complex is in a free state or bonded to the zwitterionic or the cationic polymer, and only slightly lower (*ca.* 25%) with respect to that of the well-established Ru(bpy)₃²⁺ reference sensitizer, suggesting that the PS properties were not affected.

Table 2. Estimated quantum yields of singlet oxygen production Φ_{Δ} and kinetic constant (k_{obs}) of the studied compounds in water and their cytotoxicity on cells in dark and upon irradiation. The effective concentration required for the reduction of the cell viability to 50% (EC₅₀) in dark and after irradiation (light), together with the phototherapeutic index (PI) of the three compounds on HeLa cells, is also included.

Compound name	k_{obs} (min ⁻¹) ^a	Φ_{Δ}	dark-EC ₅₀	light-EC ₅₀	PI ^b
[Ru(phen) ₂ (BAP)](OTf) ₂	0.0382	0.30	> 50 μ M	9 μ M	>5.5
Ru-PhenISA	0.0419	0.28	> 50 μ M	50 μ M	>1
Ru-PhenAN	0.0392	0.25	> 5 μ M	0.7 μ M	>7

^a) Photo-oxidation rate constant. ^b) PI: phototherapeutic index=dark-EC₅₀/light-EC₅₀.

Cytotoxicity and photo-cytotoxicity assays. As a next step, we tested the efficacy of the Ru complexes as PDT agents at the cellular level by carrying out some *in vitro* experiments on HeLa cells, both in dark and under visible light irradiation. First, we incubated cells with $[\text{Ru}(\text{phen})_2(\text{BAP})](\text{OTf})_2$, Ru-PhenISA or Ru-PhenAN at increasing concentrations for 24 h in 10% Fetal Bovine Serum to allow internalization. The long exposure time was chosen to allow the polymers to accumulate at the cellular level prior to irradiation and highlight differences in PDT efficacy for the different complexes. Then, after washing thoroughly to remove the excess of extracellular compounds, we either left cells in the dark or we irradiated them for 40 min by means of a LED visible light source (see Figure S15 for the emission profile that shows a series of relative maxima, from 400 to 800 nm, the light delivered with an irradiance of 23.7 mW/cm^2 intensity). Finally, we compared the cell viability of the dark and of the irradiated samples via alamar blue assay (see Experimental Part for details). The effective concentration required for the reduction of the cell viability to 50% (EC_{50}) was obtained by fitting the dose-response curves using a sigmoidal function (Figure 4 and Table 2) both in dark and after irradiation. For dark- EC_{50} we could only estimate a lower limit for each Ru-based PS since, even for the maximum Ru concentration, the dark- EC_{50} values were not achieved (Figure 4 panels a, b and c, black curves). From these data, we also calculated the lower limit phototherapeutic indexes PI ($\text{PI} = \text{dark-EC}_{50}/\text{light-EC}_{50}$) (Table 2).

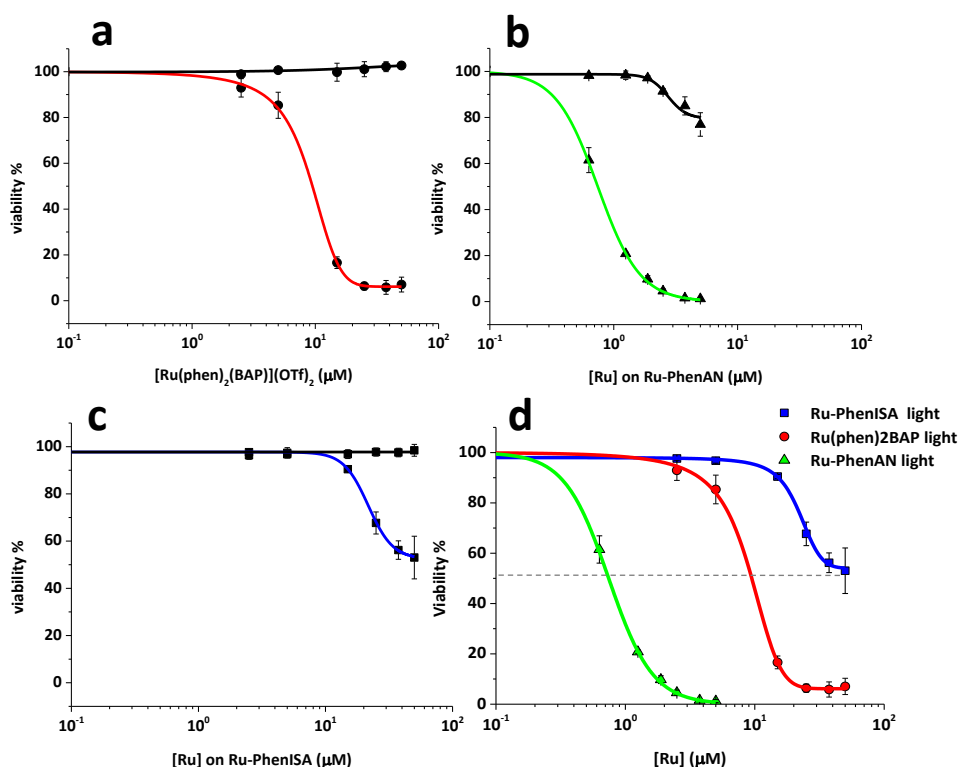


Figure 4. *In vitro* dose-response curves in the dark (black) and with visible light irradiation of HeLa cells incubated for 24 h with different concentrations of (a) $[\text{Ru}(\text{phen})_2(\text{BAP})](\text{OTf})_2$ (red curve and circles) (b) Ru-PhenAN (green curve and triangles) and (c) Ru-PhenISA (blue curve and squares), (d) superposition of the three curves with visible light irradiation. The concentrations reported in panels a-d are relative to the [Ru] content in each species (see Experimental Section for details).

In the first instance, we noticed that all the three ruthenium complexes caused cell death when irradiated by visible light: these data confirm that trisphenanthroline-based ruthenium complexes can be photoactivated even after exposure to cells, and likely after cell internalisation, making them promising PDT agents. Moreover, as already suggested by the photophysical characterization (Table 2), these results further confirmed that $\text{Ru}(\text{phen})_3^{2+}$ fragments retained photo-activity producing singlet oxygen and caused cell death after cell internalization even when conjugated to the PAA carriers. However, we noted remarkable differences in PDT efficiencies among $[\text{Ru}(\text{phen})_2(\text{BAP})](\text{OTf})_2$ and the two PAA-ruthenium counterparts, with the light- EC_{50} of the PhenAN complex lowered to $0,7 \mu\text{M}$, as opposed to $9 \mu\text{M}$ for the small $[\text{Ru}(\text{phen})_2(\text{BAP})](\text{OTf})_2$ and $50 \mu\text{M}$ for the PhenISA complex. These results clearly show that the covalent bonding of the ruthenium complex to cationic PhenAN boosts the PDT efficiency compared to the free compound, while appending it to the prevailing anionic PhenISA greatly decreases its effectiveness as a PDT agent (see the comparison of the dose-response curves with light, reported in Figure 4d). In the dark, $[\text{Ru}(\text{phen})_2(\text{BAP})](\text{OTf})_2$ and Ru-PhenISA were negligibly cytotoxic (red dots) up to the maximum tested dose ($50 \mu\text{M}$), whereas for Ru-PhenAN we noticed some toxicity, albeit much lower than that of most polycations currently in use such as PEI or PLL.^{60,61} It has been suggested that positively charged macromolecules can strongly interact, and therefore damage, the negatively charged lipid membranes of the cell.^{60,61} Because of such electrostatic interactions, it is also often believed that cationic species have higher uptake efficiency,⁶² which here could explain the higher PDT performance of Ru-PhenAN compared to the other two compounds. However, the zeta potential titration curve (Figure 2d) suggested that at physiological pH this polymer is almost neutral. Furthermore, when added to cells in the presence of biofluids such as serum, adsorption of proteins on the polymer may screen residual positive charges, making the overall complex neutral or slightly negative.⁶²⁻⁶⁵ Thus, it is difficult to clearly explain the observed toxicity in dark, likely resulting from a combination of different factors, including the cationic character of the polymer, or potentially also the nature of proteins adsorbed from serum in cell medium, among others. It is worth noting that the molecular probe $[\text{Ru}(\text{phen})_2(\text{BAP})](\text{OTf})_2$ is also positively charged, nevertheless, its toxicity in dark was lower, possibly because of a different uptake efficiency or different cationic and/or hydrophobic properties.

2.5 Uptake quantification and intracellular localization of the three Ru complexes. In order to further explain the different photo-cytotoxicity, we then moved on to assess and compare the cell internalization efficiency of the three employed ruthenium complexes. This was done by exposing HeLa cells to $[\text{Ru}(\text{phen})_2(\text{BAP})](\text{OTf})_2$, Ru-PhenISA or Ru-PhenAN for 24 h, using the same concentrations as those of the PDT assays. Flow cytometry was then used to quantify the cell fluorescence in the spectral region of the ruthenium complex emission (Figure 5). Although the emission properties may be partly affected by the subcellular localization of the compounds and, similarly, the emission quantum yield may be affected by changes in rigidity and/or lipophilicity, the cell fluorescence measured by flow cytometry can be used as an indication of the uptake efficacy of the different compounds. As expected, the cell fluorescence increased at

increasing concentration on cells, suggesting a dose dependent uptake. Interestingly, the cell fluorescence levels were very different and followed the trend Ru-PhenAN>[Ru(phen)₂(BAP)](OTf)₂>Ru-PhenISA. In particular, the fluorescence of HeLa cells treated with the cationic Ru-PhenAN was a lot higher than for both zwitterionic Ru-PhenISA and the molecular probe [Ru(phen)₂(BAP)](OTf)₂. The higher fluorescence obtained indicates much higher uptake efficacy (although other measurements like ICP-MS to determine the amount of internalized Ru would allow confirming this, excluding potential effects of the local environment on fluorescence emission), and more generally can explain the greater PDT efficiency of the cationic complex, since the ability to form singlet oxygen for PDT depends also on the efficiency to populate the triplet excitation state (thus fluorescence). Additionally, the long exposure time ensures that the fluorescence measured is mainly coming from the internalized complexes, while adhesion if present is a minor contribution^{66,67} (likely higher in proportion for cells exposed to the zwitterionic Ru-PhenISA and the smaller Ru complex, given the much lower uptake efficiency in comparison to Ru-PhenAN).

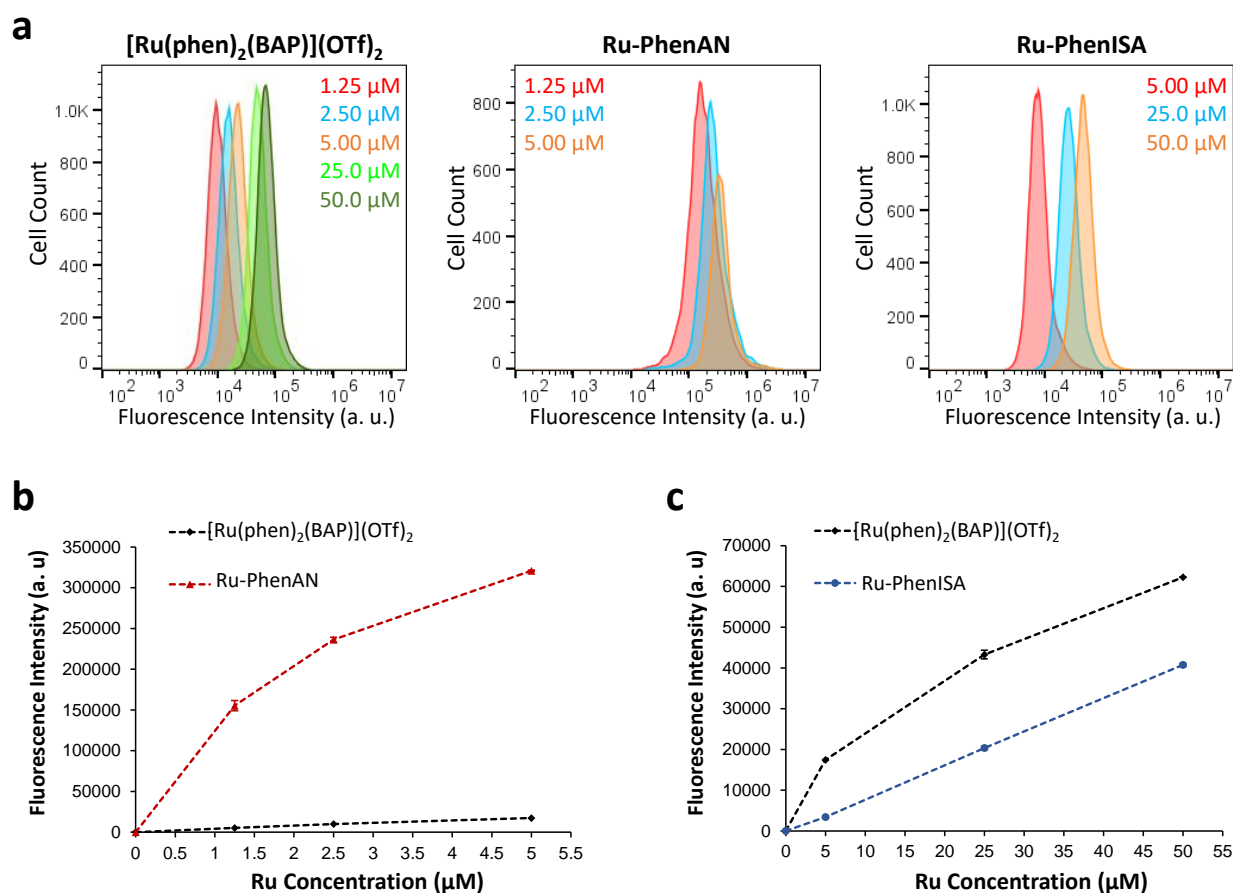


Figure 5. Cellular internalization of [Ru(phen)₂(BAP)](OTf)₂, Ru-PhenAN and Ru-PhenISA by flow cytometry. a) Fluorescence intensity distributions of HeLa cells exposed for 24 h to different concentrations of [Ru(phen)₂(BAP)](OTf)₂, Ru-PhenAN and Ru-PhenISA in complete cell culture medium. b) and c) Corresponding median fluorescence intensity values. The median fluorescence intensities of the distributions shown in panel (a) are shown as a function of the Ru concentration added to cells. Panels (b) and (c) compare the uptake of [Ru(phen)₂(BAP)](OTf)₂ and Ru-PhenAN and that of [Ru(phen)₂(BAP)](OTf)₂ and Ru-PhenISA, respectively.

As a final step, we then studied the intracellular localization of the three Ru derivatives by means of fluorescence microscopy. For cells exposed to $[\text{Ru}(\text{phen})_2(\text{BAP})](\text{OTf})_2$ and Ru-PhenISA, given the very low uptake efficiency (Figure 5), it was very difficult to clearly visualize the intracellular location of the compounds. In cells exposed to $5 \mu\text{M}$ $[\text{Ru}(\text{phen})_2(\text{BAP})](\text{OTf})_2$ the complex was detected exclusively in vesicular structures (likely vesicles of the endo-lysosomal pathways, as expected following uptake via endocytosis). Immunostaining with the lysosomal protein LAMP-1 suggested accumulation in the lysosomes (Supporting Figure S14). Ru-PhenISA treated cells, which turned out to be the least fluorescent at flow cytometry analysis, did not show any appreciable difference in their fluorescence compared to untreated control cells, even when exposed to the very high concentration of $115 \mu\text{M}$ Ru (corresponding to 1.5 mg/mL polymer concentration) (data not shown). For this reason, it was not possible to obtain clear indications on its intracellular localization. However, a previous study on HEK-293 (human embryonic kidney) cells suggested that Ru-PhenISA localizes at the cytosol level.³⁹ On the other hand, the cellular internalization of Ru-PhenAN is most peculiar: live cell imaging and overlap with the brightfield images of the cells clearly showed that few minutes after illumination at the microscope, Ru-PhenAN accumulated at nuclear level (snapshot images from live cell imaging are shown in Figure 6 and the corresponding movie is given in Supporting Movie S1). It is important to stress that previous degradation tests on PAAs of similar structure demonstrated that significant molecular weight reduction occurs under physiological conditions within several days, but never several minutes. Under the same conditions, no depolymerization reaction (retro-Michael) is observed.⁶⁸ We also confirmed the photochemical stability of this polymer complex by irradiating a sample of Ru-PhenAN in O_2 -saturated milliQ water for 2 h. The UV-vis absorption profiles resulted stable over time (Figure S16), indicating a high photostability of Ru-PhenAN in these conditions. Thus, we can exclude that the observed Ru signal inside cells comes from degraded fragments entering cells.⁴⁴ Moreover, the $\text{Ru}(\text{phen})_2^{2+}$ moiety alone does not emit fluorescence, so that we can fully exclude that it de-coordinates from the phenanthroline pendent of PhenAN, since in that case no luminescence would be observable anymore. Furthermore, since no other dyes were added to cells (for instance to stain nuclei or other cell structures), the fluorescence recorded at the nuclear level can only come from the Ru in the polymer.

Thus, the interesting cellular localization of Ru-PhenAN may suggest that this compound can escape the endo-lysosomal pathway, as noticed for other PAA polymers.^{42,69} Given the capacity of Ru to be activated by light, it is likely that this intriguing accumulation at the nuclear level might result from light-triggered effects as observed for other similar photosensitizer conjugates.⁷⁰

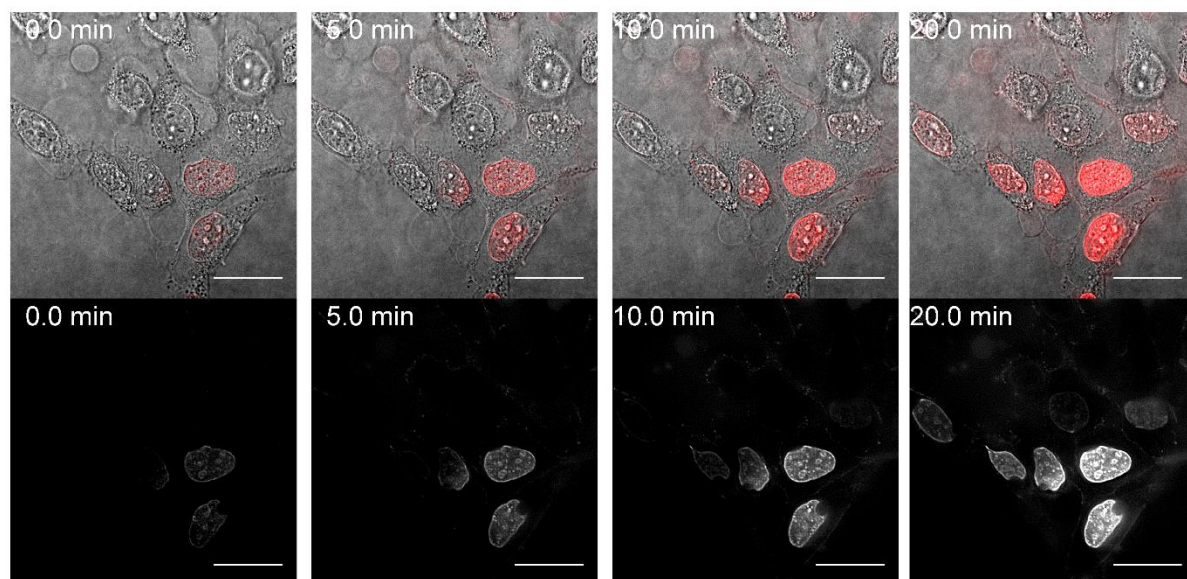


Figure 6. Cellular localization of Ru-PhenAN. Fluorescence images of HeLa cells incubated with 30 $\mu\text{g}/\text{mL}$ Ru-PhenAN in complete culture medium (cMEM) for 1 h. After 1 h exposure and removal of the extracellular Ru-PhenAN solution, cells were imaged every 30 s for a total of 20 min (see Methods for details and Supporting Movie 1 for the full movie). The fluorescence images and overlap with the brightfield channel show progressive accumulation of Ru-PhenAN at the nuclear level. Top: merged brightfield images and PhenAN-Ru fluorescence channel. Bottom: PhenAN fluorescence channel only. Scale bar: 25 μm .

Given this unique intracellular behavior, the details of the mechanisms by which this polymer is capable to reach the nucleus and in a rather short time deserve to be fully elucidated. This is far beyond the scope of this paper and it is the object of an on-going study, fully focused on this aspect. Nevertheless, nucleus-targeting photosensitizers are known to be extremely toxic upon irradiation.⁷¹ Thus the accumulation at the nuclear level, together with the higher uptake achieved by complexation with the cationic PhenAN polymer, together, can explain the greater PDT efficiency of Ru-PhenAN.

3. Conclusions

In this work, we investigated how conjugation to biocompatible polyamidoamine (PAA) polymers of different charge modulates the biological activity of a photoactive metalorganic complex ($\text{Ru}(\text{phen})_3^{2+}$).

We synthesized a molecular ($[\text{Ru}(\text{phen})_2(\text{BAP})](\text{OTf})_2$) and two macromolecular ruthenium-trisphenanthroline complexes (Ru-PhenISA and Ru-PhenAN) and compared their ability to generate singlet oxygen upon light irradiation and their use as PDT photosensitizers. In particular, the polymeric ruthenium complexes consist of an amphoteric prevailing anionic (PhenISA) and a moderately cationic (PhenAN) PAA functionalized with $\text{Ru}(\text{phen})_3^{2+}$ fragments randomly distributed less than 5% repeat units.

We then characterized photo-physically the three complexes confirming that in all cases the red triplet emitting state was able to interact by energy transfer with molecular oxygen ($^3\text{O}_2$) generating the highly cytotoxic singlet oxygen ($^1\text{O}_2$) species with comparable efficiencies.

We next ascertained the ability of the three Ru(phen)₃²⁺ complexes to cause death of HeLa cells upon visible light irradiation, and found that (cationic) Ru-PhenAN was more efficient than the (free complex and cationic) [Ru(phen)₂(BAP)](OTf)₂, which, in turn, was more efficient than (anionic) Ru-PhenISA.

Uptake quantification by flow cytometry showed that the PDT results reflected their different internalization efficiencies. Interestingly, also the intracellular localization of the three compounds differed, and this clearly plays an additional role: while [Ru(phen)₂(BAP)](OTf)₂ mostly lay confined in vesicular structures, and for Ru-PhenISA it was previously reported accumulation in the cytosol in HEK-293 (human embryonic kidney) cells,³⁹ we found that Ru-PhenAN was able to accumulate at the nuclear level, a behavior that is very unusual for similar macromolecules. The accumulation in the nucleus is likely to be one of the reasons for the remarkably higher PDT efficiency compared with both Ru-PhenISA and [Ru(phen)₂(BAP)](OTf)₂.

Overall, we believe that this work clearly shows that Ru-PhenAN is an extremely promising photosensitizer for PDT. Adding the Ru complex to the slightly cationic polyamidoamine polymer enables both much higher Ru internalization and furthermore an important accumulation at the nuclear level. These together make this compound rather unique and highly efficient in promoting cell death upon irradiation, even at rather low concentrations. Further studies beyond the scope of this paper are ongoing to fully elucidate the details of the mechanisms by which accumulation in the nucleus is achieved. Characterizing such mechanisms could enable other interesting opportunities for the use of this or similar compounds for different applications, including gene or drug delivery at the nuclear level. Thus, from a broader perspective, we believe this work also lays the foundations for the development of ruthenium-based polyamidoamine polymers with very specific pharmacological activity, where the polymer design could be tuned to achieve the desired behavior at the cell level and the ruthenium can be used for achieving targeted toxicity or other light-induced responses.

4. Experimental Section

4.1 Instruments and materials. NMR experiments were performed on a Bruker DRX400 spectrometer equipped with a Bruker 5 mm BBI Z-gradient probe head with a maximum gradient strength of 53.5 G/cm. DLS measurements were performed using a Malvern Zetasizer Nano ZS instrument at 25°C, typically dissolving samples at 1 mg/mL concentration. UV–VIS absorption spectra were acquired on an Agilent model 8543 spectrophotometer at room temperature. Size exclusion chromatography (SEC) traces were obtained with Tosoh-Haas TSK-gel G4000 PW and TSK-gel G3000 PW columns connected in series using a Waters model 515 HPLC pump equipped with a Knauer auto-sampler 3800, a light scattering (LS) Viscotek 270 dual detector, UV detector Waters model 486 operating at 230 nm, and a refractive index detector Waters model 2410. The mobile phase was a 0.1 M Tris buffer pH 8.00 (0.05 with 0.2 M sodium chloride). The flow rate was 1 mL/min and the sample concentration was 1% solutions. pH measurements were performed using an AMEL 338

pHmeter equipped with a Z113441-1EA glass microelectrode from Sigma Aldrich. Elemental C, H, N analyses were performed on a PerkinElmer CHN 2400 instrument. Polymer Ru content was determined by UV-vis analysis, by dissolving a precise amount of the compound in a known volume of milliQ water by using a volumetric flask and determining the absorbance of the ¹MLCT band at the maximum ($\lambda=458$ nm, $\epsilon_{458}=19100$). Transmission electron microscopy (TEM) images were collected using an EFTEM LEO 912AB (Zeiss). The samples suspended in water were deposited by drop casting onto copper grids (Cu-300 CK, 300 mesh), and left to naturally go to dryness for two hours. Emission spectra were obtained with an Edinburgh FLS980 spectrofluorimeter equipped with a 450 W xenon arc lamp. Emission spectra were corrected for source intensity (lamp and grating) and emission spectral response (detector and grating) by standard correction curves. Photoluminescence quantum yields were measured with a Hamamatsu Photonics absolute PL quantum yield measurement system (C11347-01 Quantaaurus spectrometer) equipped with an L11562 Xenon light source (150 W), monochromator, C7473 photonic multi-channel analyzer, integrating sphere and employing U6039-05 PLQY measurement software (Hamamatsu Photonics, Ltd., Shizuoka, Japan). Luminescent excited state lifetimes in the range from 0.5 ns to 5 μ s were measured by an Edinburgh FLS980 spectrofluorometer equipped with a TCC900 card for data acquisition in a time correlated single-photon counting experiments (0.2 ns time resolution) with a 375 nm pulsed diode. The estimated experimental errors are 2 nm on the absorption and PL bands maxima, 5% on the molar absorption coefficient, and on the luminescence quantum yield.

The photoreaction with DHN in the presence of ruthenium complexes was followed using a Jasco V-650 spectrophotometer. The experiments were performed in a 3 mL quartz cuvette inserted into a homemade housing that consists of a black box mounted on an optical bench. The irradiation source was an Osram Powerstar HCI-T with a 150 W/NDL lamp mounted on a Twin Beam T 150 R reflector that primarily emits visible light above 400 nm, with a very small emission in the 350–400 nm range that was eliminated after placing a 390 nm cutoff filter at the black box entrance. The lamp and reactor were separated by a fixed distance of 10 cm. The whole setup was maintained at ambient temperature by a continuous stream of air.

All chemicals were purchased from Sigma Aldrich and used as received, if not otherwise specified. Ultrapure water (milli-Q, Millipore, resistivity = 18 M Ω cm⁻²) was used for the preparation of the aqueous solutions. N,N'-Bis(acrylamido)acetic acid (BAC), 4-(4'-aminobutyl)-1,10-phenanthroline (BAP) and Ru(phen)₂(OTf)₂ were prepared following a literature method,³⁹ and purity was determined by NMR spectroscopy.

Immortalized HeLa cell line (from human cervix adenocarcinoma) was purchased from the American Type Culture Collection (ATCC). Minimal Essential Medium (MEM), Dulbecco modified Phosphate Buffer Saline (DPBS), Trypsin solution (porcine trypsin-EDTA 0.05%) and Fetal Bovine Serum (FBS) were purchased from Gibco Thermo Fisher Scientific. Complete medium was obtained by supplementing MEM with 10% FBS (50 ml FBS added to 500 mL MEM). Primary antibody against lysosome-associated membrane protein (LAMP-1, 1mg/mL solution) and Alexa Fluor 488 conjugated secondary antibody (2 mg/mL solution) were purchased,

respectively, from Abcam and Thermo Fisher Scientific. DNA marker 4',6-diamidino-2-phenylindole (DAPI) was purchased from Thermo Fisher Scientific. Alamar blue Cell Viability Reagent was purchased from Thermo Fisher Scientific.

Flow cytometry analyses were performed using a Beckman Coulter CYTOFLEX. Data were analyzed with FlowJo software. Forward and side scattering dot plots were used to discriminate cellular debris. A minimum of 20000 cells was acquired for each sample in order to obtain cell fluorescence intensity distributions. Three technical replicates were prepared for each sample and results are reported as the median average fluorescence and the standard deviation calculated over the three replicates. Fluorescence microscopy images were collected using a Leica TCS SP8 confocal fluorescence microscope. Live cell imaging was performed with a DeltaVision Elite microscope using a 60× oil objective. Images were analyzed with ImageJ software. Spectrofluorometric measurements of 96-well plates for the alamar blue viability assay were performed on a Molecular Devices SPECTRAmax Gemini XPS microplate spectrofluorometer. The *in vitro* photodynamic therapy tests were performed using a commercial LED lamp (MEGAMAN LED PAR16 7W GU10 SP 2800K) whose emission spectrum is reported in Figure S15.

4.2 Synthesis of the model complex [Ru(phen)₂(BAP)](OTf)₂. 7.0 mg 4-(4'-aminobutyl)-1,10-phenanthroline (BAP, 0.02788 mmol) and 16.0 mg Ru(phen)₂(OTf)₂ (0.0210 mmol) were mixed with 2 mL milli-Q water, affording a brick red suspension. Under nitrogen atmosphere and constant stirring, the system was heated at 55°C for 4h at pH 5.5 and then left at room temperature overnight. The cloudy suspension quickly homogenized and turned into a brown solution, which exhibited orange luminescence when excited by 366 nm UV light. At the end of the reaction time, pH was adjusted to 11.6 with 1M NaOH in order to precipitate unreacted Ru(phen)₂(OTf)₂, which was pelleted by centrifugation and discarded. [Ru(phen)₂(BAP)](OTf)₂ was stored as a water solution and concentration was determined via UV-vis analysis (4.15 mM). ¹H NMR (D₂O, 300 K, 9.4 T, pH 7): δ 8.46 (4H, CH(2,9) dd, J = 8.2, 1.0 Hz, and overlapped 1H, CH(9')), 8.30 (1H, CH(5') d, J = 9.2 Hz), 8.14 (1H, CH(6') d, J = 9.2 Hz), 8.11 (4H, CH(5,6) s), 7.97 (4H, CH(4,7) m and overlapped 1H, CH(7')), 7.85 (1H, CH(2') d, J = 5.3 Hz), 7.42 (4H, CH(3,8) m and overlapped 1H, CH(8')), 7.35 (1H, CH(3') d, J = 5.3 Hz), 3.18 (2H, CH₂(δ) t, J = 7.5 Hz), 2.89 (2H, CH₂(α) t, J = 6.9 Hz), 1.70 (4H, CH₂(β,γ) m). ¹³C NMR (D₂O, 300 K, 9.4 T, pH 7): δ 152.6 (CH(4,7) and CH(7')), 151.8 (CH(2')), 149.4 (CH(9')), 136.8 (CH(2,9)), 128.0 (CH(6')), 127.8 (CH(5,6)), 125.4 (CH(3')), 125.2 (CH(3,8) and CH(8')), 124.0 (CH(5')), 39.1 (CH₂(α)), 30.4 (CH₂(δ)), 26.2 (CH₂(β,γ)).

4.3 Synthesis of the zwitterionic copolymer PhenISA. N,N'-Bis(acrylamido)acetic acid (404.7 mg, 1.94 mmol, 96% purity from ¹H NMR analysis) and NaOH (86.1 mg, 1.94 mmol) were dissolved in 1.780 mL milli-Q water. pH (9-10) was assessed by a universal indicator. 4-(4'-aminobutyl)-1,10-phenanthroline (50.2 mg, 0.194 mmol, 97% purity from ¹H NMR analysis) was added. The reaction was left for 7 days at room temperature under gentle stirring, and then 2-methylpiperazine was added (178.6 mg, 1.75 mmol). The mixture was maintained under the same conditions for an additional 21 days, until the cloudy suspension

became a honey-like viscous solution. After this period, the crude reaction mixture was diluted with milli-Q water (10 mL) and acidified to pH 3 by the addition of a few drops of concentrated HCl. The water-polymer solution was then treated with an excess of morpholine (10 μ L), in order to saturate the terminal residual double bonds on the polymer. The solution was purified by ultrafiltration through a membrane with a nominal cutoff of 1000 Da and the retained portion was recovered by freeze-drying, affording a pale pink and fluffy solid. M_n = 2700 kDa, M_w = 6500 kDa, PD = 2.4.

4.4 Synthesis of the cationic copolymer PhenAN. 1,4-bisacryloil piperazine (99.7 mg, 0.514 mmol) was dissolved in 500 μ L milliQ water under an inert atmosphere, together with piperazine.(HCl)₂×2H₂O (90.7 mg, 0.465 mmol) and 4-buthilamine-1,10-phenanthroline (14.3 mg, 0.051 mmol). The concentrated suspension was stirred for 1 h at room temperature. The mixture was then warmed at 50 °C, and left to react under nitrogen for 14 days, until the cloudy suspension became a honey-like viscous solution. The as-obtained solution was then diluted by the addition of 3 mL of milliQ water and the basic pH lowered adding further aliquots of concentrated HCl until pH 3 was reached. The water-polymer solution was then treated with an excess of morpholine (5 μ L), in order to saturate the terminal residual double bonds on the polymer. The solution was purified by ultrafiltration through a membrane with a nominal cut-off of 1000 Da and the retained portion was recovered by freeze-drying, affording a pale pink and fluffy solid. M_n = 34630 kDa, M_w = 48050 kDa, PD = 1.39.

4.5 Synthesis of Ru-PhenISA. PhenISA (60 mg, 0.0113 mmol of minor monomer) was dissolved in 2.5 mL milliQ water. Ru(phen)₂(OTf)₂ (7.5 mg, 0.0099 mmol) was added to the solution and mixed. The solution was heated at 50°C for 60 minutes in a microwave reactor. After the reaction, the solution showed an intense red colour and exhibited orange luminescence when excited by 366 nm UV light. The excess Ru(phen)₂(OTf)₂ was removed by ultrafiltration through a membrane with a nominal cut-off of 3000 Da. After the purification, the solution showed a bright yellow color and its photoluminescence was preserved. The purified solution was eventually lyophilized, affording a yellow, fluffy solid (30 mg, yield 50%). Elemental analysis: Anal. Calcd for (C₁₃H₂₂N₄O₄)_{0.96}(C₄₈H₄₃N₉O₄Ru(CF₃SO₃)₂)_{0.03}(C₂₄H₂₇N₅O₄)_{0.01}(H₂O)₃ C, 44.78; H, 7.58; N, 15.29; Ru, 0.80.-Found: C, 45.10; H, 7.90; N, 14.98, Ru, 0.69. Based on number average molecular weight M_n (by SEC analysis) and the elemental analysis, the mean number of repetition units per coil is expected to be ~10, of which 0.4 contain a phen pendant, and 3 over 4 times this last one is coordinated to a Ru(phen)₂²⁺ moiety. The content of Ru per PAA mass of the sample then used for the PDT tests was determined by UV-vis spectroscopy, being known the molar extinction coefficient (ϵ = 19100 M⁻¹·cm⁻¹) for the ¹MLCT absorption peak with λ_{max} = 448-458 nm,³⁹ and resulting [Ru] = 68.4 μ M per mg/mL of lyophilized Ru-PhenISA.

4.6 Synthesis of Ru-PhenAN. PhenAN (56 mg, 0.0078 mmol of minor monomer) was dissolved in 2.5 mL milliQ water. Ru(phen)₂(OTf)₂ (6.8 mg, 0.0090 mmol) was added to the solution and mixed. The solution was heated at 50°C for 60 minutes in a microwave reactor. After the reaction, the solution showed an intense, red colour and exhibited orange luminescence when excited by 366 nm UV light. The excess Ru(phen)₂(OTf)₂

was removed by dialysis using a 10000 MWCO membrane. After the dialysis, the solution showed a bright yellow colour and its photoluminescence was preserved. The dialysed solution was eventually lyophilised, affording a yellow, fluffy solid (40 mg, yield 72%). Elemental analysis: Anal. Calcd for $(C_{14}H_{24}N_4O_2(HCl)_{1.3})_{0.95}(C_{49}H_{47}N_9O_2Ru(CF_3SO_3)_2)_{0.02}(C_{25}H_{31}N_5O_2)_{0.03}(H_2O)$ C, 49.48; H, 7.69; N, 15.82; Ru, 0.55. Found: C, 49.74; H, 7.36; N, 15.46, Ru 0.51. The content of Ru per PAA mass of the sample then used for the PDT tests was determined by UV-vis spectroscopy as for Ru-PhenISA complex, resulting $[Ru] = 53.6 \mu M$ per mg/mL of lyophilized Ru-PhenAN.

4.7 Photochemical stability of Ru-PhenAN. A sample of Ru-PhenAN was dissolved in milliQ water (1.2 mg in 5 mL H_2O) and further diluted until the most intense peak due to the absorption of the polymeric backbone showed an absorbance around 1. The solution was then bubbled with O_2 directly in a quartz cuvette for 10 min for saturating the solution. Then, the solution was irradiated using a Osram 150 W/NDL lamp (model Powerstar HCI-T), mounted on a Twin Beam T 150 R reflector, and through a cutoff optical filter (>390 nm) for 120 min overall. UV-vis absorption spectra were thus collected each 15 min during the first 60 min and the last one after a further hour irradiation (Figure S16).

4.8 Photoreaction with DHN as a test of 1O_2 production. A $1.1 \cdot 10^{-5}$ M solution of $[Ru(bpy)_3]Cl_2$ in milliQ water and a $3.3 \cdot 10^{-3}$ M solution of DHN in methanol were prepared (concentrations were determined via UV-vis analysis). The DHN solution was diluted 1:10 with the $[Ru(bpy)_3]Cl_2$ solution, to obtain a final solution of $[Ru(bpy)_3]Cl_2$ $1.0 \cdot 10^{-5}$ M and DHN $3.3 \cdot 10^{-4}$ M in water and methanol 9:1. Before the irradiation, the solution was saturated with O_2 by bubbling directly in the cuvette for 10 min. The solution was then irradiated by using a Osram 150 W/NDL lamp (model Powerstar HCI-T), mounted on a Twin Beam T 150 R reflector, and in the presence of a 390 nm through a cutoff optical filter (142 mW cm^{-2}) for a total time of 5-7 min, while absorption spectra were recorded after every 1 min of irradiation. The same procedure was adopted for the photoreaction involving $[Ru(phen)_2(BAP)](OTf)_2$, Ru-PhenISA and Ru-PhenAN, starting from $1.1 \cdot 10^{-5}$ M solutions in milliQ water (concentrations refer to the ruthenium content determined via UV-vis analysis).

4.9 Cell culture. The HeLa cell line was cultured at $37^\circ C$ with 5% CO_2 in complete MEM supplemented with non-heat inactivated FBS (50 mL added to 500 mL MEM), without antibiotics. Cultures at $\sim 80\%$ confluency were routinely split into 75 cm^2 polystyrene flasks. Splitting took place every 2-3 days.

4.10 *In vitro* photodynamic therapy. In 96-well plates, HeLa cells were seeded at a density of 7000 cells per well in 0.2 mL complete MEM. 24 h after seeding, the medium was replaced with 0.1 mL solutions of $[Ru(phen)_2(BAP)]OTf_2$, Ru-PhenISA or Ru-PhenAN in complete medium and cells were incubated for 24 h at $37^\circ C$ in a 5% CO_2 atmosphere. After 24 h exposure, the medium was carefully removed, cells were washed once with PBS and 0.05 mL complete medium was added to each well. A plate was laid 1 cm under the LED lamp (Megaman® PAR16 GU10 LR 0707-SP, Figure S15) and irradiated for 40 min ("light" plate). Meanwhile, an equivalent control plate was kept in the dark out of the incubator ("dark" plate), for the same time. After the irradiation, 0.15 mL complete medium was added to each well of both plates. Cells were further

incubated for 2 h at 37 °C in a 5% CO₂ atmosphere, after which time 20 µL alamar blue solution was added to each well. After 15 h of incubation (37 °C in 5% CO₂ atmosphere), 0.1 mL of the supernatant of each well was taken and transferred to a new plate. Plates were analysed at SPECTRAmax Gemini XPS microplate spectrofluorimeter (excitation: 560 nm, emission: 590 nm). The fluorescence intensity is directly proportional to the number of live cells. Thus, the cell viability was calculated as the ratio between the absorbance of treated cells and that of untreated control cells in the same conditions. Three replicate wells were prepared for each condition and the average fluorescence and standard deviation over the three replicates was calculated.

4.11 Uptake quantification of the Ru complexes via flow cytometry. In a 24-well plate, HeLa cells were seeded at a density of 60000 cells per well in 0.5 mL complete MEM. 24 h after seeding, the medium was replaced with 0.3 mL solution of [Ru(phen)₂(BAP)]OTf₂, Ru-PhenISA or Ru-PhenAN in complete MEM. Cells were incubated at 37 °C in a 5% CO₂ atmosphere. After 24 h exposure, wells were washed (1 x 0.5 mL complete MEM, 2 x 0.5 mL DPBS) in order to minimize the amount of compound adsorbed on the cell surface, which could affect quantification⁶⁶ of the internalized complexes. Then, the cells were harvested by incubating with 0.3 mL trypsin solution for 5 min at 37 °C. The trypsin was then inactivated by adding 0.7 mL complete MEM. The cells were pelleted by centrifuging at 250 g for 3 min and then suspended in 0.3 mL DPBS for flow cytometry analysis at a Beckman Coulter CYTOFLEX (excitation laser: 405 nm; fluorescence channel: 610/20 nm).

4.12 Intracellular localization of the Ru complexes via confocal microscopy. In a 24-well plate equipped with glass coverslips, HeLa cells were seeded at a density of 60000 cells per well in 0.5 mL complete MEM. 24 h after seeding, the medium was replaced with 0.3 mL solution of [Ru(phen)₂(BAP)]OTf₂ (5µM) in complete MEM. The cells were incubated at 37°C in a 5% CO₂ atmosphere. Then, the wells were washed (1 x 0.5 mL complete MEM, 2 x 0.5 mL DPBS). Cells were fixed by incubation with 1 mL ice-cold methanol for 5 min. Methanol was removed and lysosomes were stained with LAMP-1 primary antibody and Alexa Fluor 488 conjugated secondary antibody solutions in PBS (60 min each at room temperature). Nuclei were stained by incubating with a DAPI solution in PBS for 5 min. Coverslips were eventually mounted on glass microscope slides with a Mowiol-based mounting medium and left 24 h at room temperature in the dark, before imaging at a Leica TCS SP8 (DAPI excitation: 405 nm laser; DAPI detector: 420-460 nm. Alexa Fluor 488 excitation: 488 nm laser; Alexa Fluor 488 detector: 500-550 nm; Ruthenium complex excitation: 405 nm; Ruthenium complex detector: 600-800 nm).

4.13 Live cell imaging localization of Ru-PhenAN via confocal microscopy. HeLa cells were seeded in 35mm dish with glass coverslips (MatTek Corporation) at a concentration of 100000 cells/well. 24 h after seeding, cells were incubated with 30 or 300 µg/mL Ru-PhenAN in complete culture medium (cMEM) under standard culturing conditions (37 °C 5% CO₂) for the time indicated. Then, cells were imaged every 30 s for a total of 20 min with a DeltaVision Elite microscope and a 60X oil objective. A FITC excitation filter (461-489 nm) and

a TRITC emission filter (574.5-619 nm) were used for imaging Ru-PhenAN and polarized light was used for highlight cells structure (brightfield). Data were processed using ImageJ Software.

Associated content

Supporting Information

The Supporting Information is available free of charge on the ACS Publications website at <http://pubs.acs.org>. Multinuclear NMR spectra, titration and speciation curves for PhenAN, confocal microscopy images and movie.

Author Information

Corresponding Authors

* E-mail address: a.salvati@rug.nl

* E-mail address: daniela.maggioni@unimi.it

† Present address: Department of Chemical Engineering and Biotechnology, University of Cambridge, Philippa Fawcett Dr, Cambridge, UK

Notes

The authors declare no competing financial interest.

Acknowledgements

A.S. kindly acknowledges the University of Groningen for funding (Rosalind Franklin Fellowship). Fluorescence imaging was performed at the UMCG Microscopy and Imaging Center of the University Medical Centre Groningen. Klaas Sjollemma is acknowledged for support with confocal and live cell fluorescence imaging. Catharina Reker-Smit is kindly acknowledged for technical support. D.M. kindly acknowledges the University of Milan for funding (Transition Grant 2015-2017 - Linea 1A Progetto "Unimi Partenariati H2020").

References

- 1 DeRosa, M. Photosensitized Singlet Oxygen and Its Applications. *Coord. Chem. Rev.* **2002**, 233–234, 351–371.
- 2 Triesscheijn, M.; Baas, P.; Schellens, J. H. M.; Stewart, F. A. Photodynamic Therapy in Oncology. *Oncologist* **2006**, 11, 1034–1044.

- 3 Thota, S.; Rodrigues, D. A.; Crans, D. C.; Barreiro, E. J. Ru(II) Compounds: Next-Generation Anticancer Metallotherapeutics? *J. Med. Chem.* **2018**, *61*, 5805–5821.
- 4 van Straten, D.; Mashayekhi, V.; de Bruijn, H. S.; Oliveira, S.; Robinson, D. J. Oncologic Photodynamic Therapy: Basic Principles, Current Clinical Status and Future Directions. *Cancers (Basel)*. **2017**, *9*, 1–54.
- 5 Allison, R. R.; Downie, G. H.; Cuenca, R.; Hu, X. H.; Childs, C. J. H.; Sibata, C. H. Photosensitizers in Clinical PDT. *Photodiagnosis Photodyn. Ther.* **2004**, *1*, 27–42.
- 6 Dolmans, D. E. J. G. J.; Fukumura, D.; Jain, R. K. Photodynamic Therapy for Cancer. *Nat. Rev. Cancer* **2003**, *3*, 380–387.
- 7 Allison, R. R.; Moghissi, K. Photodynamic Therapy (PDT): PDT Mechanisms. *Clinc. Endosc.* **2013**, *46*, 24–29.
- 8 Allison, R. R.; Mota, H. C.; Sibata, C. H. Clinical PD/PDT in North America: An Historical Review. *Photodiagnosis Photodyn. Ther.* **2004**, *1*, 263–277.
- 9 Wang, S.; Gao, R.; Zhou, F.; Selke, M. Nanomaterials and Singlet Oxygen Photosensitizers: Potential Applications in Photodynamic Therapy. *J. Mater. Chem.* **2004**, *14*, 487–493.
- 10 Fan, W.; Huang, P.; Chen, X. Overcoming the Achilles' Heel of Photodynamic Therapy. *Chem. Soc. Rev.* **2016**, *45*, 6488–6519.
- 11 Lv, Z.; Wei, H.; Li, Q.; Su, X.; Liu, S.; Zhang, K. Y.; Lv, W.; Zhao, Q.; Li, X.; Huang, W. Achieving Efficient Photodynamic Therapy under Both Normoxia and Hypoxia Using Cyclometalated Ru(II) Photosensitizer through Type I Photochemical Process. *Chem. Sci.* **2018**, *9*, 502–512.
- 12 McKenzie, L. K.; Bryant, H. E.; Weinstein, J. A. Transition Metal Complexes as Photosensitizers in One- and Two-Photon Photodynamic Therapy. *Coord. Chem. Rev.* **2019**, *379*, 2–29.
- 13 Monroe, S.; Colón, K. L.; Yin, H.; Roque, J.; Konda, P.; Gujar, S.; Thummel, R. P.; Lilge, L.; Cameron, C. G.; McFarland, S. A. Transition Metal Complexes and Photodynamic Therapy from a Tumor-Centered Approach: Challenges, Opportunities, and Highlights from the Development of TLD1433. *Chem. Rev.* **2019**, *119*, 797–828.
- 14 Chen, Y.; Guan, R.; Zhang, C.; Huang, J.; Ji, L.; Chao, H. Two-Photon Luminescent Metal Complexes for Bioimaging and Cancer Phototherapy. *Coord. Chem. Rev.* **2016**, *310*, 16–40.
- 15 Zeng, L.; Gupta, P.; Chen, Y.; Wang, E.; Ji, L.; Chao, H.; Chen, Z.-S. The Development of Anticancer Ruthenium(II) Complexes: From Single Molecule Compounds to Nanomaterials. *Chem. Soc. Rev.* **2017**, *46* (19), 5771–5804.
- 16 Mari, C.; Pierroz, V.; Gasser, G. Chemical Science Combination of Ru (II) Complexes and Light: New Frontiers in Cancer Therapy. *Chem. Sci.* **2015**, *6*, 2660–2686.

- 17 Heinemann, F.; Karges, J.; Gasser, G. Critical Overview of the Use of Ru(II) Polypyridyl Complexes as Photosensitizers in One-Photon and Two-Photon Photodynamic Therapy. *Acc. Chem. Res.* **2017**, *50* (11), 2727–2736.
- 18 Poynton, F. E.; Bright, S. A.; Blasco, S.; Williams, D. C.; Kelly, J. M.; Gunnlaugsson, T. The Development of Ruthenium(II) Polypyridyl Complexes and Conjugates for *in Vitro* Cellular and *in Vivo* Applications. *Chem. Soc. Rev.* **2017**, *46* (24), 7706–7756.
- 19 Lemerrier, G.; Four, M.; Chevreux, S. Two-Photon Absorption Properties of 1,10-Phenanthroline-Based Ru(II) Complexes and Related Functionalized Nanoparticles for Potential Application in Two-Photon Excitation Photodynamic Therapy and Optical Power Limiting. *Coord. Chem. Rev.* **2018**, *368*, 1–12.
- 20 Hess, J.; Huang, H.; Kaiser, A.; Pierroz, V.; Blacque, O.; Chao, H.; Gasser, G. Evaluation of the Medicinal Potential of Two Ruthenium(II) Polypyridine Complexes as One- and Two-Photon Photodynamic Therapy Photosensitizers. *Chem. - A Eur. J.* **2017**, *23* (41), 9888–9896.
- 21 Zhang, P.; Pei, L.; Chen, Y.; Xu, W.; Lin, Q.; Wang, J.; Wu, J.; Shen, Y.; Ji, L.; Chao, H. A Dinuclear Ruthenium(II) Complex as a One- and Two-Photon Luminescent Probe for Biological Cu²⁺ Detection. *Chem. - A Eur. J.* **2013**, *19* (46), 15494–15503.
- 22 Eriksson, M.; Leijon, M.; Hiort, C.; Norden, B.; Graeslund, A. Minor Groove Binding of [Ru(phen)₃]²⁺ to [d(CGCGATCGCG)]₂ Evidenced by Two-Dimensional Nuclear Magnetic Resonance Spectroscopy. *J. Am. Chem. Soc.* **1992**, *114*, 4933–4934.
- 23 Pierroz, V.; Rubbiani, R.; Gentili, C.; Patra, M.; Mari, C.; Gasser, G.; Ferrari, S. Dual Mode of Cell Death upon the Photo-Irradiation of a Ru II Polypyridyl Complex in Interphase or Mitosis. *Chem. Sci.* **2016**, *7* (9), 6115–6124.
- 24 Mari, C.; Pierroz, V.; Rubbiani, R.; Patra, M.; Hess, J.; Spingler, B.; Oehninger, L.; Schur, J.; Ott, I.; Salassa, L.; Ferrari, S.; Gasser, G. DNA Intercalating Ru II Polypyridyl Complexes as Effective Photosensitizers in Photodynamic Therapy. *Chem. - A Eur. J.* **2014**, *20* (44), 14421–14436.
- 25 Foster, S. J.; Garcia-Lara, J.; Smythe, C.; Battaglia, G.; Thomas, J. A.; Gill, M. R. A Ruthenium(II) Polypyridyl Complex for Direct Imaging of DNA Structure in Living Cells. *Nat. Chem.* **2009**, *1*, 662–667.
- 26 Puckett, C. A.; Barton, J. K. Fluorescein Redirects a Ruthenium - Octaarginine Conjugate to the Nucleus. *J. Am. Chem. Soc.* **2009**, *131*, 8738–8739.
- 27 Puckett, C. A.; Barton, J. K. Targeting a Ruthenium Complex to the Nucleus with Short Peptides. *Bioorg. Med. Chem.* **2010**, *18*, 3564–3569.
- 28 Rodica-Mariana, I. Photodynamic Nanomedicine Strategies in Cancer Therapy and Drug Delivery (Chapter 9) In *Advances in Bioengineering*; Ed. BoD-Books on Demand, 2015 ISBN 9535121413, 9789535121411.

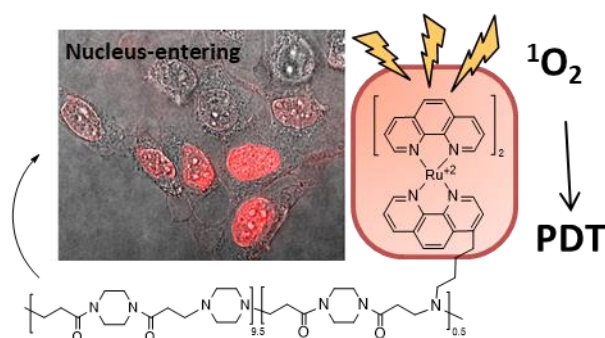
- 29 Golombek, S. K.; May, J.-N.; Theek, B.; Appold, L.; Drude, N.; Kiessling, F.; Lammers, T. Tumor Targeting via EPR: Strategies to Enhance Patient Responses. *Adv. Drug Deliv. Rev.* **2018**, *130*, 17–38.
- 30 Maeda, H.; Wu, J.; Sawa, T.; Matsumura, Y.; Hori, K. Tumor Vascular Permeability and the EPR Effect in Macromolecular Therapeutics: A Review. *J. Control. Release* **2000**, *65*, 271–284.
- 31 Villemin, E.; Ong, Y.C.; Thomas, C. M.; Gasser, G. Polymer Encapsulation of Ruthenium Complexes for Biological and Medicinal Applications. *Nature. Rev. Chem.* **2019**, *3*, 261-282.
- 32 Ferruti, P. Poly(Amidoamine)s: Past, Present, and Perspectives. *J. Polym. Sci. Part A Polym. Chem.* **2013**, *51*, 2319–2353.
- 33 Ranucci, E.; Manfredi, A. Polyamidoamines: Versatile Bioactive Polymers with Potential for Biotechnological Applications. *Chem. Africa* **2019**, *2*, 167-193.
- 34 Cavalli, R.; Bisazza, A.; Bussano, R.; Trotta, M.; Civra, A.; Lembo, D.; Ranucci, E.; Ferruti, P. Poly(amidoamine)-Cholesterol Conjugate Nanoparticles Obtained by Electrospraying as Novel Tamoxifen Delivery System *J. Drug Targeting* **2011**, *2011*, Article ID 587604, 9 pages.
- 35 Urbán, P.; Valle-Delgado, J.J.; Mauro, N.; Marques, J.; Manfredi, A.; Rottmann, M.; Ranucci, E.; Ferruti, P.; Fernández-Busquets, X. Use of poly(amidoamine) drug conjugates for the delivery of antimalarials to Plasmodium *J. Contr. Release* **2014**, *177*, 84-95.
- 36 Martí Coma-Cros, E.; Biosca, A.; Marques, J.; Carol, L.; Urbán, P.; Berenguer, D.; Riera, M.C.; Delves, M.; Sinden, R.E.; Valle-Delgado, J.J.; Spanos, L.; Siden-Kiamos, I.; Pérez, P.; Paaijmans, K.; Rottmann, M.; Manfredi, A.; Ferruti, P.; Ranucci, E.; Fernández-Busquets, X. Polyamidoamine Nanoparticles for the Oral Administration of Antimalarial Drugs *Pharmaceutics* **2018**, *10*, 225-245.
- 37 Almulathanon, A.A.Y.; Ranucci, E.; Ferruti, P.; Garnett, M.C.; Bosquillon, C. Comparison of Gene Transfection and Cytotoxicity Mechanisms of Linear Poly(amidoamine) and Branched Poly(ethyleneimine) Polyplexes. *Pharm. Res.* **2018**, *35*, 86-98.
- 38 Cavalli, R.; Primo, L.; Sessa, R.; Chiaverina, G.; Di Blasio, L.; Alongi, J.; Manfredi, A.; Ranucci, E.; Ferruti, P. The AGMA1 polyamidoamine mediates the efficient delivery of siRNA. *J. Drug Targeting* **2017**, *25*, 891-898.
- 39 Maggioni, D.; Fenili, F.; D'Alfonso, L.; Donghi, D.; Panigati, M.; Zanoni, I.; Marzi, R.; Manfredi, A.; Ferruti, P.; D'Alfonso, G. Luminescent Rhenium and Ruthenium Complexes of an Amphoteric Poly (Amidoamine) Functionalized with 1, 10-Phenanthroline. *Inorg. Chem.* **2012**, *51*, 12776–12788.
- 40 Ferruti, P.; Mauro, N.; Falciola, L.; Pifferi, V.; Bartoli, C.; Gazzarri, M.; Chiellini, F.; Ranucci, E. Amphoteric, Prevalingly Cationic L-Arginine Polymers of Poly(amidoamino acid) Structure: Synthesis, Acid/Base Properties and Preliminary Cytocompatibility and Cell-Permeating Characterizations *Macromol. Biosci.* **2014**, *14*, 390–400.
- 41 Richardson, S. C. W.; Patrick, N. G.; Lavignac, N.; Ferruti, P.; Duncan, R. Intracellular Fate of Bioresponsive Poly(Amidoamine)s in Vitro and in Vivo. *J. Control. Release* **2010**, *142*, 78–88.

- 42 Richardson, S.; Ferruti, P.; Duncan, R. Poly(Amidoamine)s as Potential Endosomolytic Polymers: Evaluation In Vitro and Body Distribution in Normal and Tumour-Bearing Animals. *J. Drug Target.* **1999**, *6*, 391–404.
- 43 Ferruti, P.; Ranucci, E.; Trotta, F.; Gianasi, E.; Evagorou, E. G.; Wasil, M.; Wilson, G.; Duncan, R. Synthesis, Characterisation and Antitumour Activity of Platinum(II) Complexes of Novel Functionalised Poly(Amido Amine)s. *Macromol. Chem. Phys.* **1999**, *200*, 1644–1654.
- 44 Ranucci, E.; Spagnoli, G.; Ferruti, P.; Sgouras, D.; Duncan, R. Poly(Amidoamine)s with Potential as Drug Carriers: Degradation and Cellular Toxicity. *J. Biomater. Sci. Polym. Ed.* **1991**, *2*, 303–315.
- 45 Ranucci, E.; Ferruti, P.; Lattanzio, E.; Manfredi, A.; Rossi, M.; Mussini, P. R.; Chiellini, F.; Bartoli, C. Acid-Base Properties of Poly(Amidoamine)s. *J. Polym. Sci. Part A Polym. Chem.* **2009**, *47*, 6977–6991.
- 46 Maggioni, D.; Galli, M.; D'Alfonso, L.; Inverso, D.; Dozzi, M. V.; Sironi, L.; Iannacone, M.; Collini, M.; Ferruti, P.; Ranucci, E.; D'Alfonso, G. A Luminescent Poly(Amidoamine)–Iridium Complex as a New Singlet-Oxygen Sensitizer for Photodynamic Therapy. *Inorg. Chem.* **2015**, *54*, 544–553.
- 47 Torres, A. S.; Maloney, D. J.; Tate, D.; Saad, Y.; MacDonnell, F. M. Retention of Optical Activity During Conversion of Λ -[Ru(1,10-phenanthroline)₃]²⁺ to Λ -[Ru(1,10-phenanthroline-5,6-dione)₃]²⁺ and Λ -[Ru(dipyrido[*a*:3,2-*h*:27,37-*c*]-phenazine)₃]²⁺. *Inorganica Chim. Acta* **1999**, *293*, 37–43.
- 48 Donghi, D.; Maggioni, D.; D'Alfonso, G.; Amigoni, F.; Ranucci, E.; Ferruti, P.; Manfredi, A.; Fenili, F.; Bisazza, A.; Cavalli, R. Tricarbonyl-Rhenium Complexes of a Thiol-Functionalized Amphoteric Poly(Amidoamine). *Biomacromolecules* **2009**, *10*, 3273–3282.
- 49 Ranucci, E.; Suardi, M. A.; Annunziata, R.; Ferruti, P.; Chiellini, F.; Bartoli, C. Poly(amidoamine) Conjugates with Disulfide-Linked Cholesterol Pendants Self-Assembling into Redox-Sensitive Nanoparticles. *Biomacromolecules*, **2008**, *9*, 2693–2704.
- 50 Ferruti, P.; Ranucci, E.; Sartore, L.; Bignotti, F.; Marchisio, M. A.; Bianciardi, P.; Veronese, F. M. Recent Results on Functional Polymers and Macromonomers of Interest as Biomaterials or for Biomaterial Modification. *Biomaterials* **1994**, *15*, 1235–1241.
- 51 De Levie, R. General Expressions for Acid-Base Titrations of Arbitrary Mixtures. *Anal. Chem.* **1996**, *68*, 585–590.
- 52 Khalili, F.; Henni, A.; East, A. L. L. pKa Values of Some Piperazines at (298, 303, 313, and 323) K. *J. Chem. Eng. Data* **2009**, *54*, 2914–2917.
- 53 Crea, F.; Crea, P.; Robertis, A. De; Sammartano, S.; Inorganica, C.; Analitica, C.; Sperone, S.; Agata, M. V. S. Thermodynamic Study for the Protonation of Branched Poly (Ethylenimine) in NaCl (Aq) and Its Dependence on Ionic Strength. *J. Chem. Eng. Data* **2007**, *52*, 279–285.
- 54 Burke, S. E.; Barrett, C. J. pH-Responsive Properties of Multilayered Poly (L -Lysine)/ Hyaluronic Acid Surfaces. *Biomacromolecules* **2003**, *4*, 1773–1783.

- 55 Wong, K.; Sun, G.; Zhang, X.; Dai, H.; Liu, Y.; He, C.; Leong, K. W. PEI-g-Chitosan, a Novel Gene Delivery System with Transfection Efficiency Comparable to Polyethylenimine in Vitro and after Liver Administration in Vivo. *Bioconjug. Chem.* **2006**, *17*, 152–158.
- 56 Given that the number average molecular weight of PhenAN is $M_n = 34630$ Da (by SEC, see Experimental Part), and that the mean molecular weight of the repeating units for the polymer containing the 5% of the minority part is ~ 290 Da, this means that, on average, each coil contains ~ 120 repeating units, of which ~ 6 are ascribable to the phen-containing moiety and only 2-3 of them bonded to a $\text{Ru}(\text{phen})_2^{2+}$ unit (that is 2% of the repeating units).
- 57 Juris, A.; Balzani, V.; Barigelletti, F.; Campagna, S.; Belser, P.; von Zelewsky, A. Ru(II) Polypyridine Complexes: Photophysics, Photochemistry, Electrochemistry, and Chemiluminescence. *Coord. Chem. Rev.* **1988**, *84*, 85–277.
- 58 Takizawa, S.; Aboshi, R.; Murata, S. Photooxidation of 1,5-Dihydroxynaphthalene with Iridium Complexes as Singlet Oxygen Sensitizers. *Photochem. Photobiol. Sci.* **2011**, *10*, 895–903.
- 59 Galli, M.; Moschini, E.; Dozzi, M. V.; Arosio, P.; Panigati, M.; D'Alfonso, L.; Mantecca, P.; Lascialfari, A.; D'Alfonso, G.; Maggioni, D. SPIO@SiO₂-Re@PEG Nanoparticles as Magneto-Optical Dual Probes and Sensitizers for Photodynamic Therapy. *RSC Adv.* **2016**, *6*, 38521–38532.
- 60 Lv, H.; Zhang, S.; Wang, B.; Cui, S.; Yan, J. Toxicity of Cationic Lipids and Cationic Polymers in Gene Delivery. *J. Control. Release* **2006**, *114*, 100–109.
- 61 Pack, D. W.; Hoffman, A. S.; Pun, S.; Stayton, P. S. Design and Development of Polymers for Gene Delivery. *Nat. Rev. drug Discov.* **2005**, *4*, 581–593.
- 62 Thompson, M.; Nel, A. E.; Somasundaran, P.; Mädler, L.; Klaessig, F.; Velegol, D.; Hoek, E. M. V.; Castranova, V.; Xia, T. Understanding Biophysicochemical Interactions at the Nano–Bio Interface. *Nat. Mater.* **2009**, *8*, 543–557.
- 63 Xia, T.; Kovichich, M.; Liong, M.; Zink, J. I.; Nel, A. E. Cationic Polystyrene Nanosphere Toxicity Depends on Cell-Specific Endocytic and Mitochondrial Injury Pathways. *ACS Nano* **2008**, *2*, 85–96.
- 64 Wang, F.; Yu, L.; Monopoli, M. P.; Sandin, P.; Mahon, E.; Salvati, A.; Dawson, K. A. The Biomolecular Corona Is Retained during Nanoparticle Uptake and Protects the Cells from the Damage Induced by Cationic Nanoparticles until Degraded in the Lysosomes. *Nanomedicine* **2013**, *9*, 1159–1168.
- 65 Monopoli, M. P.; Åberg, C.; Salvati, A.; Dawson, K. A. Biomolecular Coronas Provide the Biological Identity of Nanosized Materials. *Nat. Nanotechnol.* **2012**, *7*, 779–786.
- 66 Salvati, A.; Nelissen, I.; Haase, A.; Åberg, C.; Moya, S.; Jacobs, A.; Alnasser, F.; Bewersdorff, T.; Deville, S.; Luch, A.; Dawson, K. A. Quantitative Measurement of Nanoparticle Uptake by Flow Cytometry Illustrated by an Interlaboratory Comparison of the Uptake of Labelled Polystyrene Nanoparticles. *NanoImpact* **2018**, *9*, 42–50.

- 67 Lesniak, A.; Salvati, A.; Santos-Martinez, M. J.; Radomski, M. W.; Dawson, K. A.; Åberg, C. Nanoparticle Adhesion to the Cell Membrane and Its Effect on Nanoparticle Uptake Efficiency. *J. Am. Chem. Soc.* **2013**, *135*, 1438-1444.
- 68 F. Bignotti, P. Sozzani, E. Ranucci and P. Ferruti, NMR Studies, Molecular Characterization, and Degradation Behavior of Poly(amido amine)s. 1. Poly(amido amine) Deriving from the Polyaddition of 2-Methylpiperazine to 1,4-Bis(acryloyl)piperazine, *Macromolecules* 1994, **27**, 7171-7178.
- 69 Griffiths, P. C.; Paul, a; Khayat, Z.; Wan, K.-W.; King, S. M.; Grillo, I.; Schweins, R.; Ferruti, P.; Franchini, J.; Duncan, R. Understanding the Mechanism of Action of Poly(Amidoamine)s as Endosomolytic Polymers: Correlation of Physicochemical and Biological Properties. *Biomacromolecules* **2004**, *5*, 1422–1427.
- 70 Ohtsuki, T.; Miki, S.; Kobayashi, S.; Haraguchi, T.; Nakata, E.; Hirakawa, K.; Sumita, K.; Watanabe, K.; Okazaki, S. The Molecular Mechanism of Photochemical Internalization of Cell Penetrating Peptide-Cargo-Photosensitizer Conjugates. *Sci. Rep.* **2016**, *5* (1), 18577.
- 71 Jakubaszek, M.; Goud, B.; Ferrari, S.; Gasser, G. Mechanisms of Action of Ru(II) Polypyridyl Complexes in Living Cells upon Light Irradiation. *Chem. Commun.* **2018**, *54*, 13040–13059.

Table of Contents



Complexation of [Ru(phen)₃] to a cationic polyamidoamine increases Ru cell uptake, achieves accumulation at the nuclear level and increases PDT efficacy.